NASA TM-80088

NASA Technical Memorandum 80088

NASA-TM-80088 19790022971

COMPARISON OF THREE-DIMENSIONAL PANEL METHODS WITH STRIP BOUNDARY-LAYER SIMULATIONS TO EXPERIMENT

Scott O. Kjelgaard and James L. Thomas

July 1979

National Aeronautics and
Space Administration

Langley Research Center
Hampton, Virginia 23665

SUMMARY

The results from several three-dimensional surface panel methods coupled on a streamwise strip basis to two-dimensional boundary-layer methods have been compared to experimental data. Several different boundary-layer simulations were investigated; the results indicated that either a transpiration or camber-line displacement simulation gave comparable boundary-layer effects which converged to the expected two-dimensional result with increasing aspect ratio. The method was applied to several varied configurations for which, in general, the lift predictions agreed well with an approximate method based on correcting the inviscid lift using the two-dimensional section viscous characteristics. The wing pressures and the effect of the boundary layer on the wing pressures were predicted with reasonable accuracy.

INTRODUCTION

At subsonic speeds, surface panel methods applicable to general configurations have been developed to evaluate the inviscid aerodynamic characteristics. Three-dimensional boundary-layer methods for general configurations have been developed but are in an early stage of development as compared to two-dimensional boundary-layer methods. Two-dimensional methods have been used extensively and require only a fraction of the computing times of the three-dimensional methods. As an initial evaluation of viscous effects on moderately high aspect-ratio wings, two-dimensional boundary-layer methods applied along streamwise strips can provide an estimate of the boundary-layer characteristics. Such methods have been developed and applied such as in references 1 to 3.

There are several different ways to simulate the boundary layer with an inviscid-flow model, including the two most common which are: (1) displacement of the inviscid surface based on the boundary-layer displacement thickness and (2) specification of non-zero normal velocities on the inviscid surface. The simulations are based on modeling the outflow at the edge of the boundary layer in the inviscid-flow solution. Both approaches are equivalent theoretically, but the second simulation is recognized as the most efficient computationally since the geometry remains unchanged, especially if considering iteration between the inviscid and boundary-layer solutions in three dimensions. However, quite different boundary-layer effects between the various simulations have been reported in the literature by previous investigators (refs. 1 to 3).

The purpose of this investigation is to compare the alternate methods of boundary-layer simulation so that these differences can be understood. Also, several inviscid panel methods coupled on a streamwise strip basis to two-dimensional boundary-layer methods are applied to several configurations to assess the prediction accuracy and sensitivities of such an approach.

SYMBOLS

AR	planform aspect ratio, b^2/S
b	wing span, m
c	chord, m
$\bar{c}$	mean aerodynamic chord, m
c_ℓ	section lift coefficient based on local chord, Section lift/$q_\infty c$
c_{ℓ_α}	section lift-curve slope, $(\partial c_\ell/\partial\alpha)$, per deg
C_L	total lift coefficient based on wing planform area, Total lift/$q_\infty S$
C_L	total lift-curve slope, $(\partial C_L/\partial\alpha)$, per deg
C_m	total pitching-moment coefficient based on wing planform area and mean aerodynamic chord, Total pitching moment/$q_\infty S\bar{c}$
C_p	pressure coefficient, $(p - p_\infty)/q_\infty$
k_2	section lift-loss ratio, two-dimensional boundary-layer lift increment divided by the two-dimensional inviscid lift, $(c_{\ell,p} - c_{\ell,v})/c_{\ell,p}$
k_3	total lift-loss ratio, three-dimensional boundary-layer lift increment divided by the three-dimensional inviscid lift, $(C_{L,p} - C_{L,v})/C_{L,p}$
k_{3a}	approximate total lift-loss ratio $(k_{3a} = k_2\, C_{L_\alpha}/c_{\ell_\alpha})$
M	Mach number
p	pressure, Pa
q	dynamic pressure, Pa
R_N	Reynolds number based on mean aerodynamic chord

S	surface distance in the streamwise direction, m or wing planform area, m^2
U	inviscid velocity magnitude, m/sec
V_N	inviscid velocity magnitude normal to the surface ($V_N = 0$ in inviscid flow; $V_N = \partial(U\delta^*)/\partial S$ using transpiration simulation)
x/c	longitudinal location, fraction of chord
x_{MC}	longitudinal moment center location, fraction of mean aerodynamic chord
z/c	airfoil coordinate perpendicular to chord line, fraction of chord
α	angle of attack, deg
δ^*	boundary-layer displacement thickness, m
Γ	planform dihedral angle, deg
η	spanwise location, fraction of semispan
λ	planform taper ratio
Λ	planform sweep angle, deg

Subscripts:

c/4	quarter chord
exp	experimental
p	inviscid result
root	root chord
v	viscous result, obtained either from experimental data or from inviscid method plus strip boundary-layer simulation
∞	free-stream conditions

Notation:

BL	boundary layer

DISCUSSION

Approximate Effect of Strip Boundary Layer

Before discussing the results comparing various boundary-layer simulations, it is useful to estimate the effect of a streamwise strip boundary-layer simulation on the lift of a three-dimensional wing. The effect of the boundary layer is generally to reduce the lift. A parameter used below to quantify that effect is the boundary-layer lift-loss ratio (k_2 in two dimensions and k_3 in three dimensions) which is the loss in lift coefficient attributed to the boundary layer divided by the inviscid lift coefficient. The k_2 and k_3 expressions are:

$$k_2 = \frac{c_{\ell,p} \quad c_{\ell,v}}{c_{\ell,p}} \quad ; \quad k_3 = \frac{C_{L,p} \quad C_{L,v}}{C_{L,p}}$$

The $c_{\ell,p}$ or $C_{L,p}$ values are obtained from an inviscid solution, and the $c_{\ell,v}$ or $C_{L,v}$ values are obtained either from experimental data or from an inviscid solution with a boundary-layer simulation.

The strip boundary-layer assumption should be valid only for wings of moderately high aspect ratio and relatively low sweep and taper. For such wings, the local Reynolds number is roughly constant across the span. Also, the chordwise pressure distribution at any span station is similar to that on the two-dimensional section if comparisons are made at the same section lift coefficient. The inputs to twodimensional boundary-layer methods consist primarily of Reynolds number and a pressure coefficient versus arc length distribution, so that the computed three-dimensional section boundary-layer characteristics would be very similar to those of the two-dimensional section, corresponding to the same section lift coefficient.

The effect of the boundary layer on the two-dimensional inviscid flow can be treated as a local uncambering effect which is a function of the section inviscid lift. On a three-dimensional wing, the two-dimensional effect of the camber change is modified by the finite wing such that the two-dimensional lift change is reduced roughly as the ratio of the three-dimensional to the two-dimensional lift-curve slope.

Under the assumption of a constant section lift coefficient spanwise, the total lift-loss ratio, k_3, can be given as a function of the two-dimensional section lift-loss ratio, k_2. The resulting approximate value of the total lift-loss ratio is denoted k_{3a} and is given as

$$k_{3a} = k_2 \frac{C_{L_\alpha}}{c_{\ell_\alpha}}$$

Thus, the total lift-loss ratio using the strip boundary-layer assumption should generally be less than the corresponding section lift-loss ratio and should converge to the section lift-loss ratio as the aspect ratio is increased. For experimental total lift-loss ratios in excess of the section lift-loss ratio, it is presumed that the assumptions of a strip boundary-layer representation are not valid for the experimental test conditions.

General Comparisons of Boundary-Layer Simulations

For two-dimensional airfoil analyses, there are a large number of computer programs available which simulate the boundary layer with an inviscid-flow model. At least three different simulations have been used including: (1) displacement of the inviscid surface a distance * normal to the surface; (2) specification of nonzero normal velocities on the inviscid surface (transpiration); and (3) displacement of the inviscid camber line only based on the * distribution. In two-dimensional applications, all of the approaches have given results in agreement with each other and with experimental data.

In three-dimensional applications, several different results have been reported in the literature (refs. 1 to 3) as described below. In reference 1, a finite-difference method for two-dimensional boundary-layer analyses was coupled to a three-dimensional potential-flow analysis method developed previously (ref. 5). Both a transpiration and surface displacement method of simulation were used with the result that the surface displacement simulation agreed best with the experimental data and produced a much higher lift loss than the transpiration simulation. The investigators of reference 2 coupled an integral method for infinite swept-wing boundary layer analyses to a potential-flow method similar to that of reference 5 except for a slightly different Kutta condition. Only the transpiration method of simulation was used, and results were obtained similar to those of reference 1 using transpiration. The investigators of reference 3 coupled an integral method for two-dimensional boundary-layer analyses to the potential-flow analysis method of reference 5. They used a transpiration simulation, but obtained boundary-layer lift losses much greater than the transpiration simulations of either reference 1 or 2. For a 45° swept-wing test case analyzed previously in both references 1 and 2, the investigators of reference 3 obtained results which agreed very well with the experimental data and the surface displacement simulation of reference 1. Reference 3 thus supposedly proved the equivalence of the transpiration and surface displacement simulations but offered no explanation for the poor results using transpiration obtained in references 1 and 2. These different results led to the present investigation.

A computer program was coded which coupled the integral method for two-dimensional boundary-layer analyses used in reference 4 to either the potential-flow panel method of reference 5 or the more recently developed method of reference 6. The purpose was to check the results in references 1 to 3, that is, the boundary-layer characteristics and the implementation of the first two simulations mentioned above. Comparisons were made with results from the computer program of reference 1. The computed boundary-layer characteristics from reference 1 were checked with calculations using the method of reference 4 and were found to be very similar. The general results of applying the various simulations to several test cases are discussed below and are followed by specific results for a 45^{o} swept-wing case analyzed in references 1 to 3.

Simulation of the boundary layer using transpiration with either of the panel methods of reference 5 or 6 gave similar results to the transpiration simulations of references 1 and 2. The predicted lift-loss ratios were in good agreement with the expected approximate result given above and agreed with a simulation based on camber-line-only displacement. Simulation of the boundary layer using surface displacement in the panel method of reference 5 gave results similar to the surface displacement simulation of reference 1 as expected; however, the predicted lift losses were much higher than the expected approximate result using the two-dimensional section characteristics.

The difference in airfoil shape between the surface displacement and camber-line displacement simulations used above consists of a thickness distribution equal to the average of the upper and lower surface displacement thicknesses; the effect of such a symmetrical thickness contribution on the lift should be small. Since the inviscid method of reference 5 has been used successfully for a number of years in analyzing airfoils of zero trailing-edge thickness a possible cause of the conflicting results is that the inviscid-flow model used in reference 5 does not account consistently for an airfoil with a finite thickness trailing edge. Such an airfoil always occurs when using the surface displacement simulation as the upper and lower surfaces are moved normal to the surface a distance equal to the upper and lower displacement thicknesses, respectively. A series of two-dimensional cases, some of which are shown below, were analyzed to investigate this possibility.

Many airfoils, such as the NACA 4-digit series of airfoils, as defined have finite thickness trailing edges. Inviscid incompressible section lift calculations at $\alpha = 5^{o}$ using the panel method (low order source) corresponding to that in reference 5 are shown in table 1 for the NACA 0012 airfoil. Results are also shown for a thinned version of that airfoil obtained by removing the trailing-edge thickness linearly as a function of x/c (thus leaving the camber line unchanged). Comparison calculations are also shown for the higher order source panel method of reference 7 and from the finite difference method of reference 8. The panel method results for the thinned version of the airfoil agree very closely with the finite difference result. The finite difference method predicts almost identical lift for the airfoil as defined and the thinned version as expected. However, both panel method results for the airfoil as defined are low; the two panel methods also seem to be converging to different values of section lift coefficient.

The NASA LS(1)-0417 airfoil section (formerly the GA(W)-1) as defined in reference 9 has a cusped, finite thickness trailing edge. Inviscid incompressible section lift calculations at $\alpha = 0^{\circ}$ are shown in table 2 for the airfoil as defined and a thinned version with the trailing-edge thickness removed as above. The panel method results for the thinned airfoil agree reasonably well with the finite difference result, but again, both panel method results for the airfoil as defined are low. The input coordinates used in the analyses are those given in reference 9; the panel method results could be improved slightly by distributing the points in a more optimum fashion, especially near the trailing edge, but it is believed such a modification would not improve the finite-thickness trailing edge results significantly.

A particular case in which the three-dimensional lift loss using surface displacement was much greater than expected was a high-aspect-ratio rectangular wing of NACA 0012 section. Two-dimensional comparisons of the different simulations are discussed below.

In order to compare the different simulations more directly, a thinned version of the NACA 0012 airfoil was analyzed using the computer program of reference 4 at a R_N of 3.0 million and $\alpha = 5^{\circ}$. The predicted inviscid lift coefficient is $c_{\ell,p} = 0.604$; the lift coefficient after multiple iterations between the inviscid and boundary-layer solutions is $c_{\ell,v} = 0.559$. The lift coefficient after a single iteration is $c_{\ell,v} = 0.545$. Note, most of the effect of the boundary layer is obtained after a single iteration as is assumed in reference 1. The defining airfoil coordinates, inviscid velocities, displacement thicknesses as computed on the first iteration from the inviscid velocities, and normal velocities corresponding to a transpiration simulation are given in table 3. Given in table 4 are the airfoil coordinates corresponding to surface-displacement and camber-line displacement simulations and which were generated using the information in table 3. Results from using the three simulations in the panel methods of references 5 and 7 are shown in table 5. Displacement simulation results using the finite difference method are also shown. All of the simulations predict section lift-loss ratios in the range of 0.07-0.12 except for the surface-displacement simulation using the panel method of reference 5. Note that for this case, the surface-displacement simulation using the higher order source panel method appears reasonable, but the results in tables 1 and 2 indicate that this may not always be the case.

For results using the panel methods of references 5 and 7, no special handling of the trailing edge was done--the gap between the upper and lower surface trailing edges was left unpaneled. An inviscid-flow model of the finite-thickness trailing edge, such as the model in reference 10 which simulates a separated-base type of flow, seems to be required for consistent results. The unpaneled gap at the trailing edge is believed to be the source of the inconsistent results using surface-displacement reported in reference 1. In three-dimensional applications, the only viable simulation choice at present seems to be the transpiration simulation. Results pertaining to the conflicting results obtained using that simulation for a particular test case are discussed in the next section.

Results for a Particular Test Case

Several previous investigators have compared three-dimensional inviscid analyses coupled with strip boundary-layer methods for a semispan wing tested by Kolbe and Bolz (ref. 11) at a R_N of 18×10^6. The wing had a quarter-chord sweep of 45^o and an aspect ratio of 3.0. The high sweep and low aspect ratio of this wing are not consistent with the assumptions inherent in a strip boundary-layer calculation; therefore, some of the excellent results in the literature are somewhat surprising.

The lift coefficient predictions from references 1 to 3 are presented in table 6 along with computed results from the present study. The results presented all assume no boundary-layer representation in the wake since the effect on the resulting lift is presumed to be small. The boundary layers are iterated with the inviscid solution until convergence in references 2 and 3 as opposed to a single iteration in reference 1 and the check program coded for the present investigation. Continued iteration can, in general, affect the results, but for this particular wing, the differences between a single and multiple iteration were checked and found to be small. (The lift loss ratio with iteration was approximately 80 percent of that computed using only a single iteration.)

As seen in table 6, there are some differences in the inviscid lift calculations arising from differences in the potential-flow panel methods. The panel representation and results from a convergence study in reference 12 are shown in figure 1 and indicate that the converged inviscid lift coefficient at $\alpha = 8.23°$ is $C_L = 0.43$. The potential-flow panel method of reference 6 is closest to the converged inviscid lift coefficient while the panel methods of references 2 and 5 are about 6 percent high for the panel density shown in figure 1 (which is typical of the densities used in refs. 1 to 3).

Considering the boundary-layer lift-loss ratios shown in table 6, the camber-line displacement simulation and all but one of the transpiration simulations agree with the approximate lift loss ratio, k_{3a}, of about 2 percent. The surface-displacement simulation using the potential-flow method of reference 1 agrees best with the experimental data but predicts an unrealistically high total lift-loss ratio of approximately 12 percent which is presumed to be attributed to the inconsistencies in the low order source modeling of a finite-thickness trailing edge. The transpiration method of reference 3 also gives an unrealistically high total lift-loss ratio although the paper describes no significant difference from the methods used in references 1 and 2 and the program coded for the present investigation. Note that the good agreement of these two results with the experimental data is fortuitous and relies on a cancellation of errors (both the initial inviscid-lift calculation and the computed lift-loss ratio are too high). Using the converged inviscid-lift coefficient of 0.43 and a strip boundary-layer lift-loss ratio of 2 percent results in a lift coefficient of 0.42 which is only slightly higher than the experimental lift coefficient of 0.41. The remaining difference is attributed at present to the three-dimensional boundary layer that actually exists on this swept wing instead of the two-dimensional boundary layer assumed.

Comparisons With Experiment

As part of an effort to determine the accuracy with which inviscid panel methods coupled with strip boundary-layer simulations can represent experimental results, several varied configurations were analyzed. All of the configurations are of fairly high aspect ratio so that the strip boundary-layer assumptions are expected to be valid. Because the experimental data were taken at relatively low Mach numbers (less than 0.3) for which compressibility effects are slight, the program calculations were done for incompressible flow ($M = 0$). Also, the boundary-layer characteristics were computed directly from the inviscid solution, as in reference 1, with no further iteration between the inviscid and boundary-layer solutions.

For most of the results presented, the analyses were performed using the available computer program of reference 1 coupled with the transpiration boundary-layer simulation. The surface displacement simulation was not used because of the difficulties discussed previously associated with the analysis of a finite thickness trailing edge. A camber-line displacement simulation was not used since it requires surface lofting and subsequent recomputation of the aerodynamic influence matrix, thus requiring considerably more computer resources than the transpiration simulation. Even when using the transpiration method of simulation, low values of lift coefficient were predicted in the initial inviscid calculations for an airfoil section with a finite-thickness trailing edge. To overcome this problem, all of the airfoil section thickness distributions were reduced linearly as a function of x/c to have zero thickness at the trailing edge.

During the course of the analyses presented below, several of the inviscid calculations using the method of reference 1 were checked for convergence either by repeating the analysis with a larger number of panels defining the surface or by using the panel method of reference 6. All of the inviscid calculations are not shown in the comparison figures below, but a summary compilation of the inviscid lift calculations is given in table 7. Additionally, the inviscid-plus-strip boundary-layer calculations made using the method of reference 1 for each of the comparison cases below are compiled in table 8. Corresponding approximate lift-loss ratios (k_{3a}) which use a section lift-loss ratio computed using the method of reference 4 are also tabulated.

The investigators of reference 13 calculated the boundary layer on an aspect-ratio-5 wing with 30° of sweep using experimentally measured pressures as input to a three-dimensional boundary-layer method. The computed boundary-layer characteristics were used to calculate transpiration simulation normal velocities which were used in a potential-flow analysis program. Strip boundary-layer calculations using the method of reference 1 are compared with the results from reference 13 in figure 2. The boundary-layer parameters computed using the strip boundary-layer method are slightly lower than the three-dimensional boundary-layer calculations. The total lift and spanload calculations with the strip boundary-layer simulation, however, agree very closely with the experimental data. The lift-loss ratio calculated using the strip boundary layer corresponds to 6 percent while that from reference 13 is approximately 10 percent.

The half-span panel representation of a semispan wing for which experimental results are reported in reference 14 is shown in figure 3. Analysis results using the method of reference 1 are shown in figure 4. The results for the panel density shown in figure 3 agree very well with the experimental data in overall force and moment. The total lift-loss ratio at $\alpha = 6.75^{\circ}$ is 0.056 which is close to the approximate lift-loss ratio, k_{3a}, of 0.043. A camber line displacement simulation was also used for this case, and the resulting boundary-layer lift loss was almost identical with the transpiration simulation results. The surface displacement simulation of reference 1 resulted in a lift loss of 16 percent, considerably more than even the two-dimensional section lift loss.

Inviscid calculations were made with double the number of spanwise panels, and the resulting spanload is shown in figure 4(b). The effect of doubling the spanwise panel number is to reduce the spanload, principally at the outboard sections, so that the inviscid spanload outboard of $\eta = 0.85$ is below the experimental data. The tip vortex separation ahead of the trailing edge causes a local increase in spanload near the tip which is not accounted for in the potential-flow method. Additionally, the limited size of the reflection plane used in the experiment may be causing some difference at the inboard end.

Results using the panel method of reference 6 and the two-dimensional boundary-layer method of reference 4 are shown in figure 5. The inviscid lift is 4 percent lower than that predicted by the method of reference 1, being caused by a lower spanload outboard such as obtained by doubling the number of spanwise panels in the method of reference 1. However, the total boundary-layer lift loss ratio is nearly the same. The results in figure 5 show clearly the underestimation of the spanload at the tip and the subsequent underprediction of total lift.

The full-span panel representation of a wing-body for which experimental data are available from references 15 and 16 is presented in figure 6. Both the experimental and the analysis results using the method of reference 1 are shown in figure 7. The predicted effect of the boundary layer is very slight; the lift-curve slope even with the transpiration boundary-layer simulation is much higher than the experimental data. However, the predicted chordwise pressure distribution agrees very well with the experimental data; the agreement is much more than the total lift comparison would indicate. No boundary-layer and/or separation effects on bodies were modeled in any of the results presented in this report, which may be the cause of these differences between theory and experiment.

The full-span panel representation of the Advanced Technology Light Twin (ATLIT) wing-body-nacelle configuration is shown in figure 8. Experimental results from reference 17 and analysis results using the method of reference 1 for the wing-alone configuration are shown in figure 9. The total lift and moment predictions agree very closely with the experimental data up to a lift coefficient of 0.7 beyond which trailing-edge separation effects (which are not modeled) become evident.

Comparisons of theoretical with experimental results for the wing-body-nacelle configuration are presented in figure 10. The experimental data are from recent tests in the Langley full-scale tunnel facility (ref. 18); the total force and moment data are from balance readings and the spanwise loads are obtained from pressure integrations. The experimental pressures and spanloads are for the wing-body-nacelle configuraton with propellers stopped and with the aircraft as built. A series of modifications were made to the configuration during the wind-tunnel tests to reduce the drag; lift and moment tail-off data for this fully clean version estimated from tail-on data are shown in figure 10(a). The fully clean data agrees more closely with the theoretical predictions. The analysis method overpredicts the experimental lift although the stability parameter $\partial C_m/\partial C_L$ and the spanwise variation of the load are predicted reasonably well. The experimental load on the nacelle is low because it represents an integration over only the forward portion. The predicted total lift loss ratio at $\alpha = 4.0$ is 0.6 which is about half of the two-dimensional lift loss (0.12) expected for this high-aspect-ratio wing.

Experimental results from reference 19 and analysis results using the method of reference 1 are shown in figure 11 for a wing-body similar to that of the ATLIT. The theoretical results agree reasonably well with the experimental data and the computed lift-loss ratio is close to the approximate lift loss ratio (table 8).

The full-span panel representation of the aspect-ratio-10 Energy Efficient Transport (EET) wing-body configuration tested in the Langley V/STOL tunnel (ref. 20) is shown in figure 12. A comparison of the analysis results with the experimental data are shown in figure 13. The force and moment results agree with the experimental data although there is a significant zero lift pitching-moment difference. The chordwise pressure distributions are predicted quite well except on the lower surface. Because of the strong favorable pressure gradient at the lower trailing-edge surface for this supercritical airfoil, the boundary layer computed on the single iteration of the result presented is probably lower than that which would be predicted by successive iterations and may be the cause of the disagreement. The predicted effect of the boundary layer on the lift agrees reasonably well with the approximate lift loss based on the two-dimensional section characteristics.

An aspect-ratio-10 configuration obtained by adding tip extensions and a horizontal tail is shown in figure 14 and the analysis and experimental results are shown in figure 15. The effect of the horizontal tail on the lift and pitching-moment slope is well predicted. The agreement in zero lift pitching moment may be somewhat fortuitous because of the zero lift moment disagreement shown in figure 13 for the tail-off configuration. The predicted and experimental chordwise pressures on the wing are very similar to those on the aspect-ratio-10 configuration.

CONCLUDING REMARKS

The results of coupling different strip boundary-layer simulations with inviscid surface panel methods indicate either a transpiration or camber-line displacement simulation predicts boundary-layer effects generally in accordance with expected results. The transpiration simulation is, of course, preferred since the geometry remains unchanged and the aerodynamic influence matrix need not be recomputed. The surface-displacement simulation gives rise to a finite-thickness trailing edge for which inconsistent results were obtained; an improved treatment probably requires incorporation of a separated base-flow trailing-edge model. Correlation with the experimental data has indicated mixed results. The predicted lift loss, however, agrees reasonably well with an approximate lift loss based on correcting the inviscid lift using the two-dimensional airfoil section characteristics. The pressures on the wing surfaces and the effects of the boundary layer on the pressures generally seem to be predicted with reasonable accuracy.

REFERENCES

1. Hess, John L.: A Fully Automated Combined Potential-Flow Boundary-Layer Procedure for Calculated Viscous Effects on the Lifts and Pressure Distributions of Arbitrary Three-Dimensional Configurations. Rept. No. MDC J7491, McDonnell-Douglas Corp., June 1977

2. Dvorak, F. A.; Woodward, F. A.; and Maskew, B.: A Three-Dimensional Viscous/Potential Flow Interaction Analysis Method for Multi-Element Wings. NASA CR 152012, 1977

3. Lemmerman, L. A.; an Sonnad, V. R.: Three-Dimensional Viscous-Inviscid Coupling Using Surface Transpiration. J. Aircraft, vol. 16, no. 6, June 1979, pp. 353

4. Morgan, Harry L., Jr.: A Computer Program for the Analysis of Multielement Airfoils in Two-Dimensional Subsonic, Viscous Flow. NASA SP 347, pt. II, pp. 713-747, 1975

5. Hess, John L.: Calculation of Potential Flow About Arbitrary Three Dimensional Lifting Bodies. Rept. No. MDC J5679-01, McDonnell-Douglas Corp., October 1972

6. Ehlers, F. E.; Epton, M. A.; Johnson, F. T.; Magnus, A. E.; and Rubbert, P. E.: An Improved Higher Order Panel Method for Linearized Supersonic Flow. AIAA Paper 78-15, 1978

7. Hess, John L.: Higher-Order Numerical Solutions of the Integral Equation for the Two-Dimensional Neumann Problem. Computer Methods in Applied Mechanics and Engineering, vol. 12, no. 1, February 1973, pp. 1-15

8. Bauer, F.; Garabedian, P.; and Korn, D.: Supercritical Wing Sections III. Lecture Notes in Economics and Mathematical Systems, vol. 150, Springer-Verlag, New York, 1977

9. McGhee, Robert J.; and Beasley, William D.: Low-Speed Aerodynamic Characteristics of a 17-Percent Thick Airfoil Section Designed for General Aviation Applications. NASA TN D-7428, 1973

10. Kemp, William B., Jr.: A Vector-Continuous Loading Concept for Aerodynamic Panel Methods. NASA TM 80104, 1979

11. Kolbe, Carl D.; and Boltz, Frederick W.: The Forces and Pressure Distribution at Subsonic Speeds on a Plane Wing Having 45° of Sweepback, An Aspect Ratio of 3, and a Taper Ratio of 0.5. NACA RM A51G31, 1951

12. Thomas, James L.; and Miller, David S.: Numerical Comparisons of Panel Methods at Subsonic and Supersonic Speeds. AIAA Paper 79-0404, 1979

13. Piers, W. J.; Schipholt, G. J.; and van den Berg, B.: Calculation of the Flow Around a Swept Wing, Taking Into Account the Effect of the Three-Dimensional Boundary Layer. Part 1: Wing With Turbulent Boundary Layer. NLR TR 75076, National Aerospace Laboratory NLR, 1975

14. Yip, Long P.; and Shubert, Garl L.: Pressure Distributions on a 1- by 3 Meter Semispan Wing at Sweep Angles from 0° to 40° in Subsonic Flow. NASA TN D-8307, 1976

15. Mineck, Raymond E.; and Schwendemann, Myles F.: Aerodynamic Characteristics of a Vectored-Thrust V/STOL Fighter in the Transition-Speed Range. NASA TN D-7191, 1973

16. Mineck, Raymond E.; and Margason, Richard J.: Pressure Distribution on a Vectored-Thrust V/STOL Fighter in the Transition-Speed Range. NASA TM X-2867, 1974

17. Wentz, W. H., Jr.; and Volk, C. G., Jr.: Reflection-Plane Tests of Spoilers on an Advanced Technology Wing With a Large Fowler Flap. NASA CR 2696, 1976

18. Yip, Long P.: Comparison of Wing Pressure Distributions and Boundary-Layer Characteristics for the Advanced Technology Light Twin-Engine Airplane (ATLIT) With Two-Dimensional Section Data for the GA(W)-1 Airfoil. NASA CP 2046, vol. II, pp. 33-44, 1978

19. Morgan, Harry L., Jr.; and Paulson, John W., Jr.: Aerodynamic Characteristics of Wing-Body Configuration With Two Advanced General Aviation Airfoil Sections and Simple Flap Systems. NASA TN D-8524, 1977

20. Morgan, Harry L., Jr.: Model Geometry Description and Pressure Distribution Data From Tests of EET High-Lift Research Model Equipped With Full-Span Slat and Part-Span Flaps. NASA TM 80048, 1979

Table 1

Comparisons of Inviscid Calculations for NACA 0012 Airfoil at $\alpha = 5.0^{\circ}$

Airfoil	Panels	Trailing Edge Half Thickness/ Chord	Low Order Source Method (Ref. 1)	Higher Order Source Method (Ref. 7)	Finite Difference Method (Ref. 8)
			c_{ℓ}	c_{ℓ}	c_{ℓ}
NACA 0012 as defined	40	0.00126	0.553	0.569	--
	70	.00126	.549	.571	--
	98	.00126	.548	.576	0.602
NACA 0012 modified	40	0	.596	.596	--
	70	0	.599	.598	--
	98	0	.600	.599	.603

Table 2

Comparison of Inviscid Calculations for LS(1)-0417 Airfoil at $\alpha = 0^{\circ}$

Airfoil	Panels	Trailing Edge Half Thickness/ Chord	Low Order Source Method (Ref. 1) c_{ℓ}	Higher Order Source Method (Ref. 7) c_{ℓ}	Finite Difference Method (Ref. 8) c_{ℓ}
LS(1)-0417 as defined	74	0.00355	0.494	0.438	0.569
LS(1)-0417 modified	74	0	.556	.539	.569

Table 3

Airfoil Coordinates and Inviscid/Boundary-Layer Calculations From Method of Reference 4 for Thinned Version of NACA 0012 Airfoil;
$\alpha = 5^{o}$; $R_N = 3.0 \times 10^6$; $c_{\ell,p} = 0.604$

Lower surface						Upper surface					
Panel Edge	x/c	z/c	U/U_∞	δ^*/c	V_N/U_∞*	Panel Edge	x/c	z/c	U/U_∞	δ^*/c	V_N/U_∞*
1	1.00000	0.00000	.86530	.00360	.01323	35	.00272	.00909	1.62866	.00006	.00378
2	.98000	-.00278	.89000	.00320	.00762	36	.01029	.01726	1.74785	.00008	.00478
3	.95768	-.00584	.91028	.00294	.00712	37	.02173	.02449	1.70416	.00012	.00362
4	.91535	-.01140	.94143	.00252	.00443	38	.03636	.03090	1.64006	.00016	-.00312
5	.87349	-.01663	.95863	.00228	.00344	39	.05358	.03654	1.58273	.00013	.00804
6	.83071	-.02172	.97020	.00210	.00291	40	.07318	.04150	1.53482	.00024	.00707
7	.78693	-.02667	.97902	.00195	.00286	41	.09467	.04579	1.49475	.00035	.00630
8	.74387	-.03130	.98631	.00181	.00248	42	.11796	.04944	1.46002	.00046	.00286
9	.70051	-.03571	.99230	.00169	.00259	43	.14286	.05251	1.42957	.00052	.00372
10	.65779	-.03979	.99735	.00157	.00273	44	.16911	.05500	1.40241	.00060	.00445
11	.61630	-.04349	1.00159	.00145	.00252	45	.19663	.05694	1.37741	.00070	.00414
12	.57461	-.04694	1.00529	.00134	.00240	46	.22532	.05833	1.35392	.00080	.00475
13	.53456	-.04996	1.00850	.00124	.00254	47	.25516	.05921	1.33130	.00092	.00398
14	.49605	-.05256	1.01086	.00114	.00236	48	.28644	.05961	1.30996	.00103	.00459
15	.45834	-.05479	1.01251	.00105	.00245	49	.31843	.05954	1.28961	.00116	.00428
16	.42153	-.05663	1.01342	.00096	.00257	50	.35164	.05901	1.26987	.00129	.00435
17	.38612	-.05803	1.01343	.00087	.00238	51	.38612	.05803	1.25050	.00143	.00409
18	.35164	-.05901	1.01231	.00079	.00219	52	.42153	.05663	1.23144	.00157	.00448
19	.31843	-.05954	1.00973	.00072	.00230	53	.45834	.05479	1.21289	.00173	.00423
20	.28644	-.05961	1.00544	.00065	.00140	54	.49605	.05256	1.19472	.00189	.00430
21	.25516	-.05921	.99946	.00061	.00150	55	.53456	.04996	1.17672	.00206	.00455
22	.22532	-.05833	.99114	.00057	.00227	56	.57461	.04694	1.15853	.00225	.00422
23	.19663	-.05694	.97962	.00051	.00308	57	.61630	.04349	1.14060	.00244	.00460
24	.16911	-.05500	.96415	.00043	.00284	58	.65779	.03979	1.12250	.00265	.00478
25	.14286	-.05251	.94362	.00036	.00294	59	.70051	.03571	1.10412	.00286	.00496
26	.11796	-.04944	.91663	.00029	.00306	60	.74387	.03130	1.08506	.00313	.00541
27	.09467	-.04579	.88047	.00022	.00278	61	.78693	.02667	1.06469	.00341	.00612
28	.07318	-.04150	.83043	.00016	.00319	62	.83071	.02172	1.04286	.00374	.00775
29	.05358	-.03654	.75963	.00009	-.00055	63	.87349	.01663	1.01732	.00416	.01114
30	.03636	-.03090	.65252	.00012	.00190	64	.91535	.01140	.98617	.00477	.02257
31	.02173	-.02449	.47950	.00010	.00265	65	.95768	.00584	.93524	.00606	.03734
32	.01029	-.01726	.17328	.00007	.00265	66	.98000	.00278	.90400	.00720	.05601
33	.00272	-.00909	.37525	.00006	.00350	67	1.00000	0.00000	.86530	.00885	0.00000
34	0.00000	0.00000	1.11570	.00005	.00442						

*Value given at panel edge i corresponds to value at midpoint of panel between edges i and i + 1

Table 4

Airfoil Coordinates Used in Surface Displacement/Camber Line Displacement Simulations for Thinned Version of NACA 0012; $R_N = 3.0 \times 10^6$; $c_{\ell,p} = 0.604$

Lower surface				Upper surface			
Panel Edge	x/c	(z/c)*	(z/c)**	Panel Edge	(x/c)	(z/c)*	(z/c)**
1	1.00000	-.00362	.00261	35	.00267	.00912	.00910
2	.98000	-.00600	.00010	36	.01024	.01732	.01726
3	.96000	-.00852	-.00254	37	.02167	.02460	.02446
4	.91600	-.01386	-.00815	38	.03630	.03105	.03082
5	.87377	-.01889	-.01345	39	.05354	.03666	.03633
6	.83095	-.02381	-.01863	40	.07313	.04173	.04128
7	.78714	-.02861	-.02370	41	.09461	.04613	.04555
8	.74406	-.03310	-.02846	42	.11790	.04990	.04916
9	.70068	-.03739	-.03303	43	.14280	.05303	.05214
10	.65793	-.04135	-.03725	44	.16906	.05560	.05454
11	.61642	-.04493	-.04109	45	.19659	.05764	.05641
12	.57472	-.04828	-.04470	46	.22529	.05913	.05773
13	.53465	-.05120	-.04787	47	.25514	.06013	.05854
14	.49612	-.05370	-.05061	48	.28643	.06064	.05886
15	.45840	-.05584	-.05298	49	.31844	.06070	.05872
16	.42157	-.05759	-.05496	50	.35167	.06030	.05811
17	.38615	-.05890	-.05649	51	.38617	.05946	.05705
18	.35166	-.05980	-.05761	52	.42160	.05820	.05557
19	.31844	-.06026	-.05828	53	.45843	.05652	.05366
20	.28644	-.06026	-.05848	54	.49617	.05445	.05136
21	.25515	-.05982	-.05823	55	.53471	.05201	.04868
22	.22530	-.05890	-.05750	56	.57479	.04918	.04560
23	.19660	-.05745	-.05622	57	.61651	.04592	.04208
24	.16907	-.05543	-.05438	58	.65803	.04243	.03833
25	.14282	-.05287	-.05198	59	.70079	.03958	.03421
26	.11792	-.04973	-.04899	60	.74420	.03441	.02978
27	.09463	-.04601	-.04542	61	.78730	.03006	.02515
28	.07314	-.04166	-.04120	62	.83114	.02544	.02026
29	.05355	-.03663	-.03629	63	.87399	.02076	.01531
30	.03632	-.03101	-.03079	64	.91600	.01613	.01042
31	.02168	-.02458	-.02444	65	.96000	.01170	.00572
32	.01025	-.01731	-.01725	66	.98000	.00998	.00388
33	.00267	-.00912	-.00910	67	1.00000	.00883	.00261
34	-.00005	0.00000	0.00000				

*Surface displacement simulation airfoil coordinates
**Camber line displacement simulation airfoil coordinates

Table 5

Comparisons of Boundary-Layer Simulations for Thinned Version of NACA 0012 Airfoil Using Boundary-Layer Parameters From the Method of Reference 4; $R_N = 3.0 \times 10^6$

			Inviscid + Boundary Layer					
		Inviscid	Transpiration Simulation		Camber-Line Displacement Simulation		Surface Displacement Simulation	
Method	α	$c_{\ell,p}$	$c_{\ell,v}$	k_2	$c_{\ell,v}$	k_2	$c_{\ell,v}$	k_2
Low order source (ref. 5)	5.05	0.604	0.558	0.08	0.532	0.12	0.483	0.20
Higher order source (ref. 7)	5.06	.604	.563	.07	.550	.09	.544	.10
Finite difference (ref. 8)	5.01	.604	--	--	.536	.11	.536	.11
Modified Oeller (ref. 4)	5.00	.604	--	--	.545	.10	--	--

Table 6

Comparison of Three-Dimensional Lift Coefficient Predictions Inviscid Flow and With Several Strip Boundary-Layer Simulations for the Wing Tested in Reference 11

$\alpha = 8.23°$, $R_N = 18 \times 10^6$, $C_{L,exp} = 0.41$, $k_2 = 0.05$, $k_{3a} = 0.02$

Inviscid Flow	Inviscid + Transpiration Simulation		Inviscid + Surface Displacement Simulation		Inviscid + Camber-Line Displacement Simulation		
$C_{L,p}$	$C_{L,v}$	k_3	$C_{L,v}$	k_3	$C_{L,v}$	k_3	Method
0.458	0.449	0.019	0.405	0.116	-----	-----	Ref. 1
.46	.45	.02	-----	-----	-----	-----	Ref. 2
.455	.415	.087	-----	-----	-----	-----	Ref. 3
.458	.453	.012	.402	.122	.452	0.013	Inviscid method of ref. 5 + BL method of ref. 4
.432	.426	.014	-----	-----	-----	-----	Inviscid method of ref. 6 + BL method of ref. 4

Table 7

Summary of Inviscid-Lift Calculations

Configuration	No. of Panels	Method	$(C_L)_{\alpha=0}$	C_{L_α}
AR=5 semispan wing (fig. 2)	30x12 30x7	ref. 5 ref. 6	-0.123 - .124	0.072 .071
AR=6 semispan wing (fig. 3)	40x8 40x16 40x9	ref. 5 ref. 5 ref. 6	0 0 0	.080 .078 .077
ATLIT semispan wing (fig. 8)	50x10 50x20 50x11	ref. 5 ref. 5 ref. 6	.453 .450 .473	.098 .097 .096
AR=5 wing-body (fig. 6)	30x9-176	ref. 5	- .055	.090
AR=9 wing-body (fig. 11)	50x9-176	ref. 5	.413	.098
AR=10 wing-body (fig. 12)	40x7-198 40x14-198	ref. 5 ref. 5	.371 .364	.105 .103
ATLIT wing-body-nacelle (fig. 8)	50x8-160-192	ref. 5	.464	.106
AR=12 wing-body-tail (fig. 14)	40x8-258-36x3	ref. 5	.326	.124

*Wing or tail surface panel numbers given as chordwise number x spanwise number

Table 8

Comparison of Computed Three-Dimensional Lift-Loss Ratio (k_3) With An Approximate Lift-Loss Ratio (k_{3a})

Configuration	Streamwise	$R_N x 10^{-6}$	$C_{L,p}$	$C_{L,v}$*	(k_3)*	k_{3a}	k_2**
AR=3 semispan wing (fig. 1)	NACA 64A010 to c/4	18 4	.457 .457	.449 .444	.02 .03	.02 .03	.04 .07
AR=5 semispan wing (fig. 2)	NACA 0012-64	1.4	.307	287	.06	.07	.12
AR=6 semispan wing (fig. 3)	NACA 0012	3.2	.539	.509	.06	.04	.06
ATLIT semispan wing (fig. 8)	LS(1)-0417	1.0 1.0	.453 .847	.384 .778	.16 .08	.17 .13	.21 .16
AR=5 wing-body (fig. 6)	NACA 63A010	1.1	.305 .665	.297 .641	.03 .04	.04 .05	.05 .06
AR=9 wing-body (fig. 11)	LS(1)-0417	1.5	.413 .805	.347 .757	.16 .06	.17 .13	.22 .17
AR=10 wing-body (fig. 12)	Supercritical	1.4 1.4	.371 .814	.315 .749	.15 .08	.19 .11	.22 .12
ATLIT wing-body-nacelle (fig. 8)	LS(1)-0417	3.5 3.5	.464 .890	.416 .838	.11 .06	.15 .11	.17 .12

*Computed using the computer program of reference 1
**Computed using the computer program of reference 4

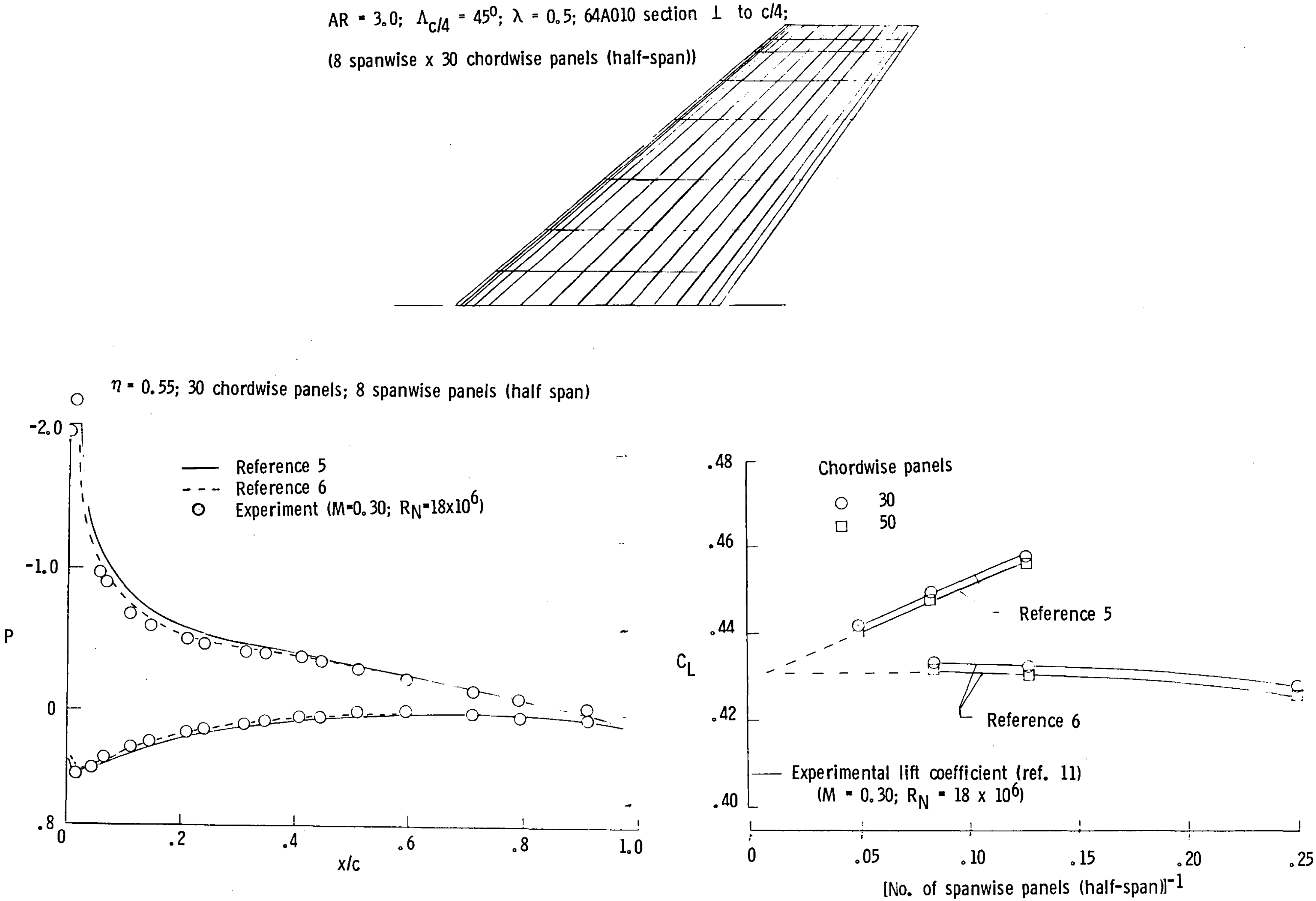

Figure 1.- Convergence characteristics and comparisons of inviscid calculations with experiment of reference 11; M = 0; α = 8.23°.

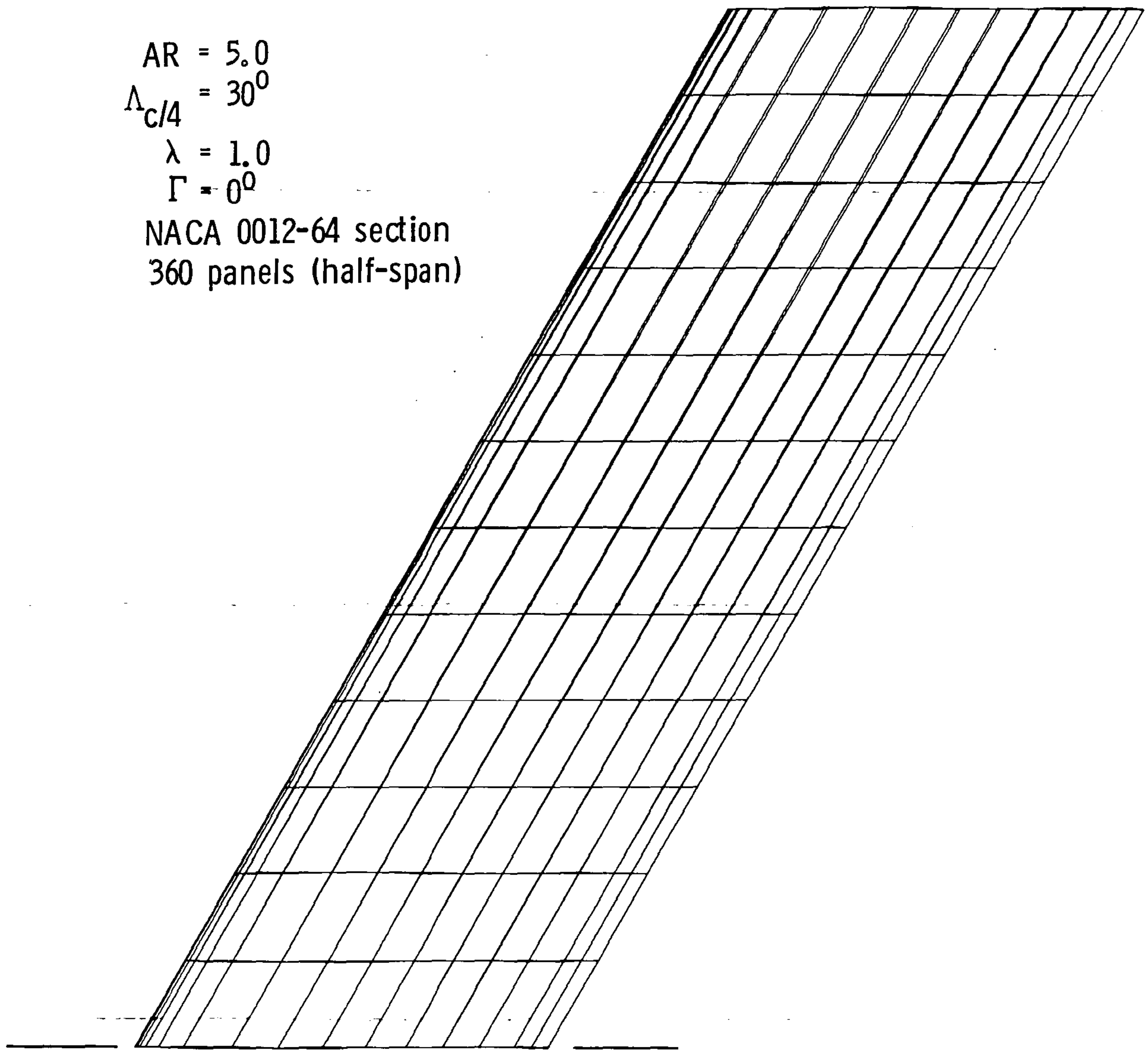

(a) Top view of half-span panel representation of semispan wing

Figure 2 .- Comparison of inviscid with strip boundary calculations of reference 1 to inviscid with 3-D boundary-layer calculations of reference 13.

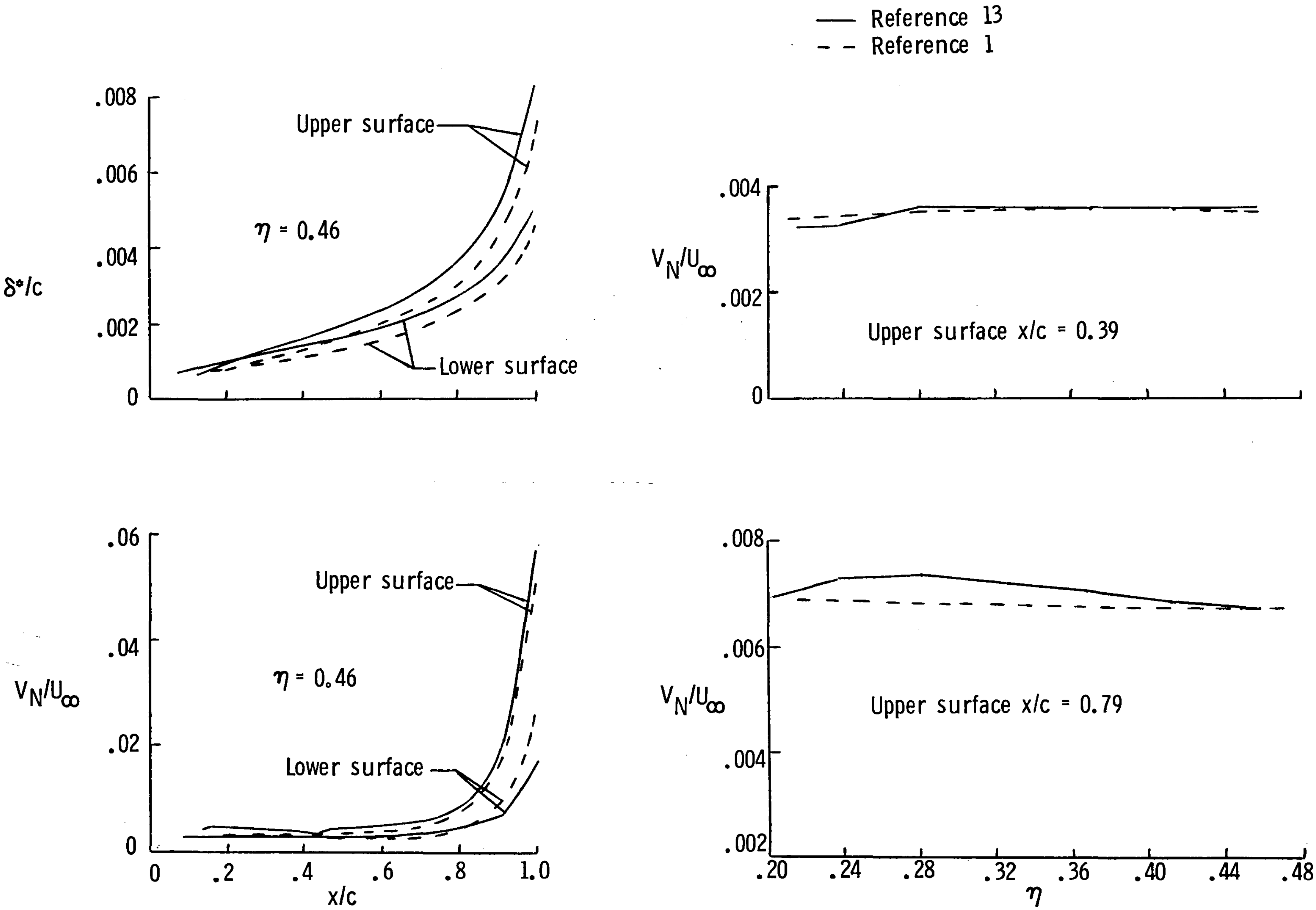

(b) Comparison of boundary-layer simulation parameters; $\alpha = 6^0$; $R_N = 1.4 \times 10^6$

Figure 2.- Continued.

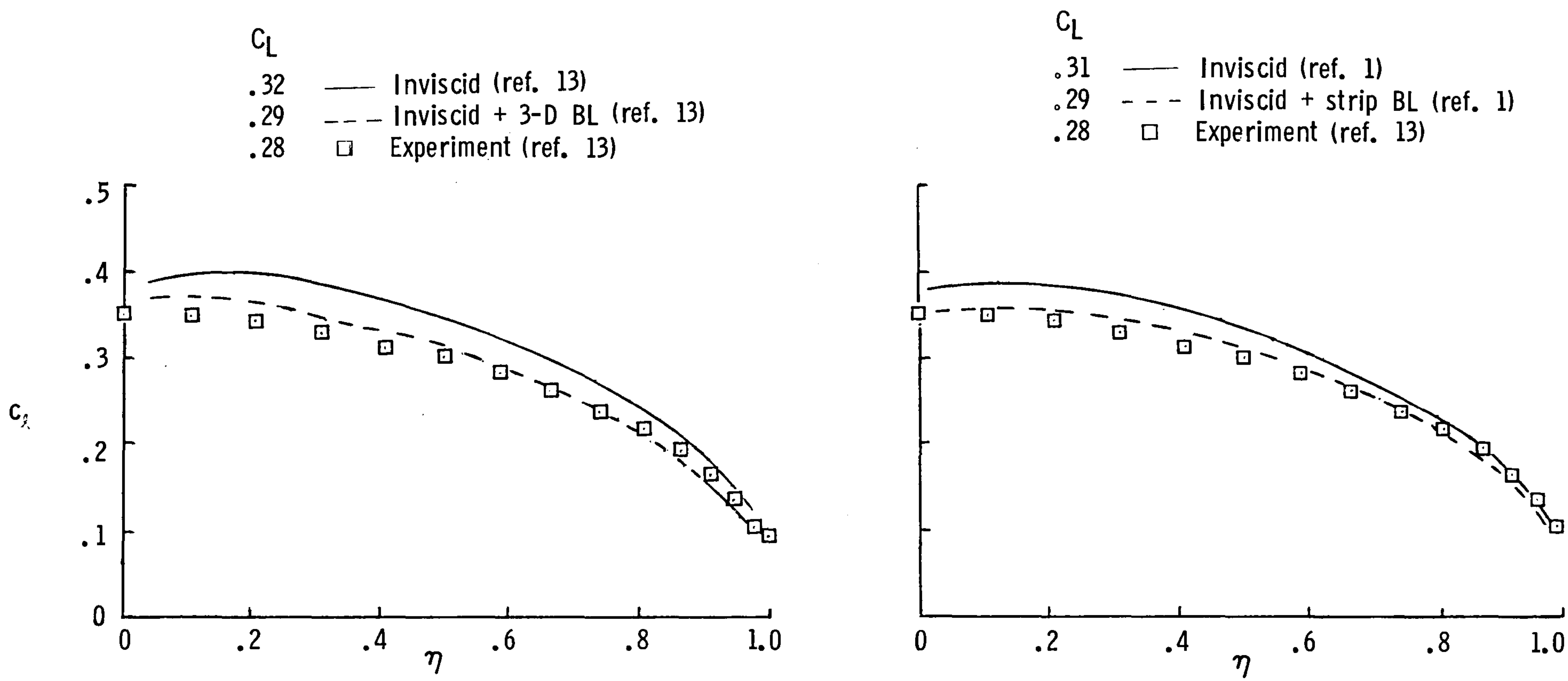

(c) Total lift and span load comparisons; $\alpha = 6^0$; $R_N = 1.4 \times 10^6$

Figure 2.- Concluded.

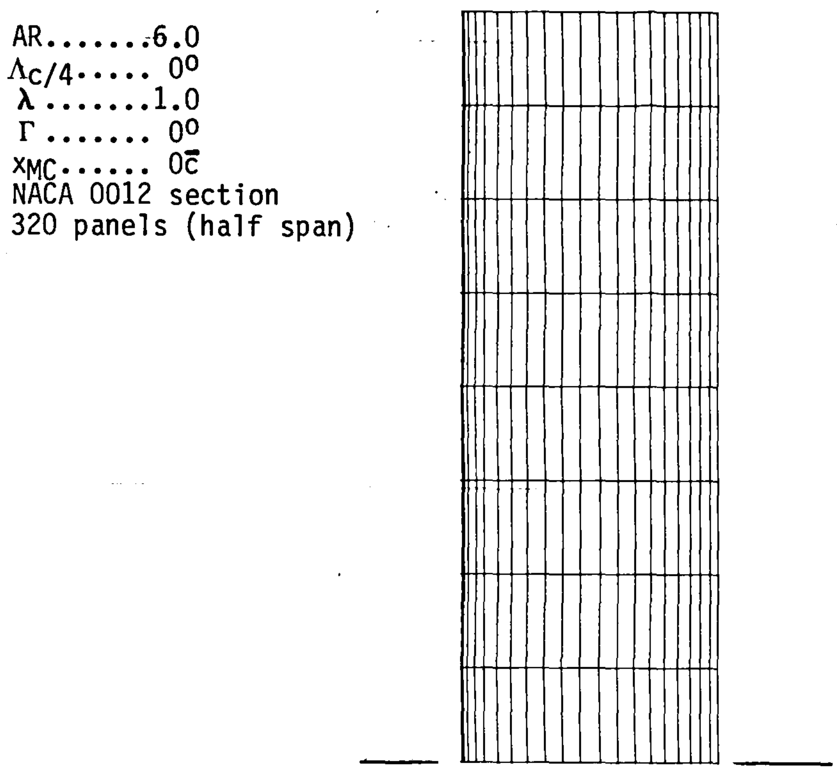

Figure 3.- Top view of half-span panel representation of wing tested in reference 14.

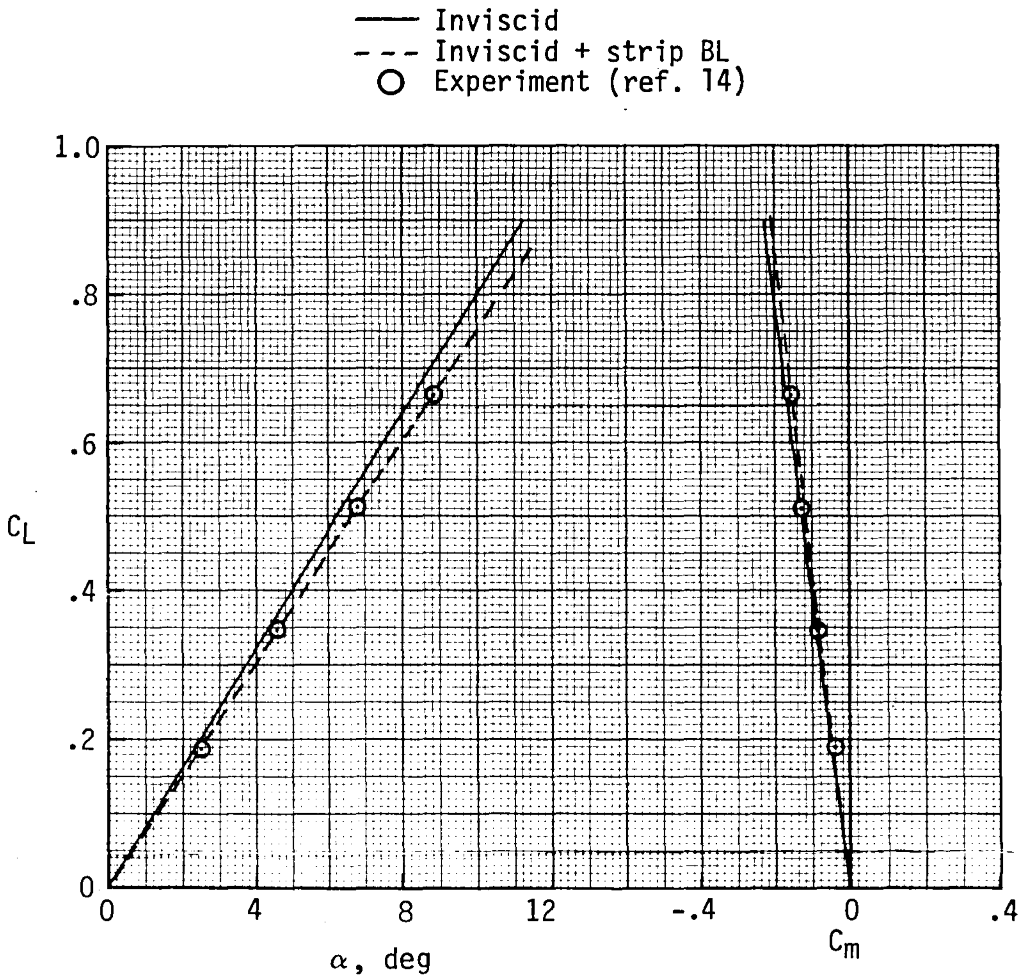

(a) Total lift and pitching moment characteristics

Figure 4.- Comparisons with experiment of wing-alone results using the method of reference 1. $M = 0.1$; $R_N = 3.2 \times 10^6$.

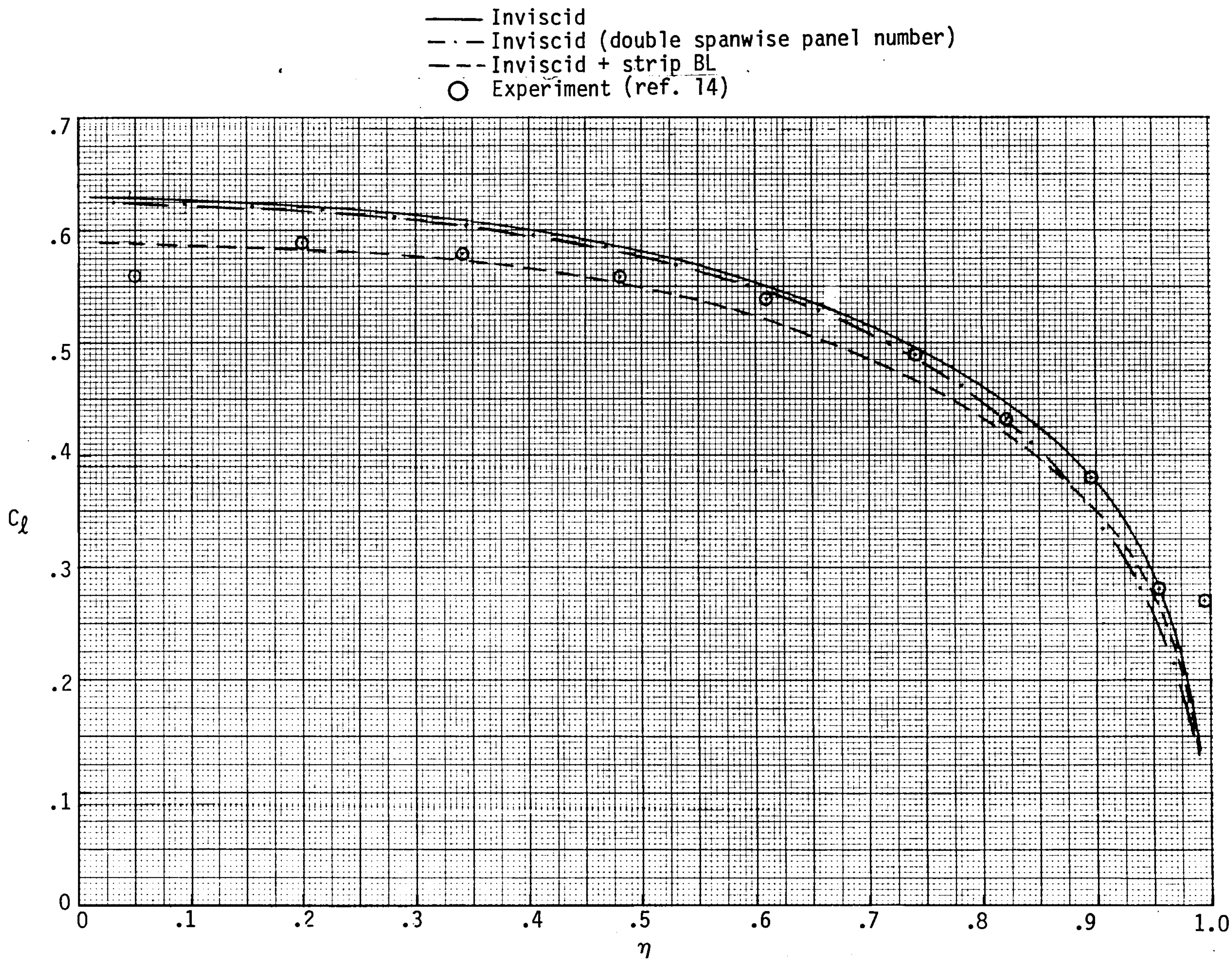

(b) Spanwise load variation, $\alpha = 6.75^{\circ}$

Figure 4.- Continued.

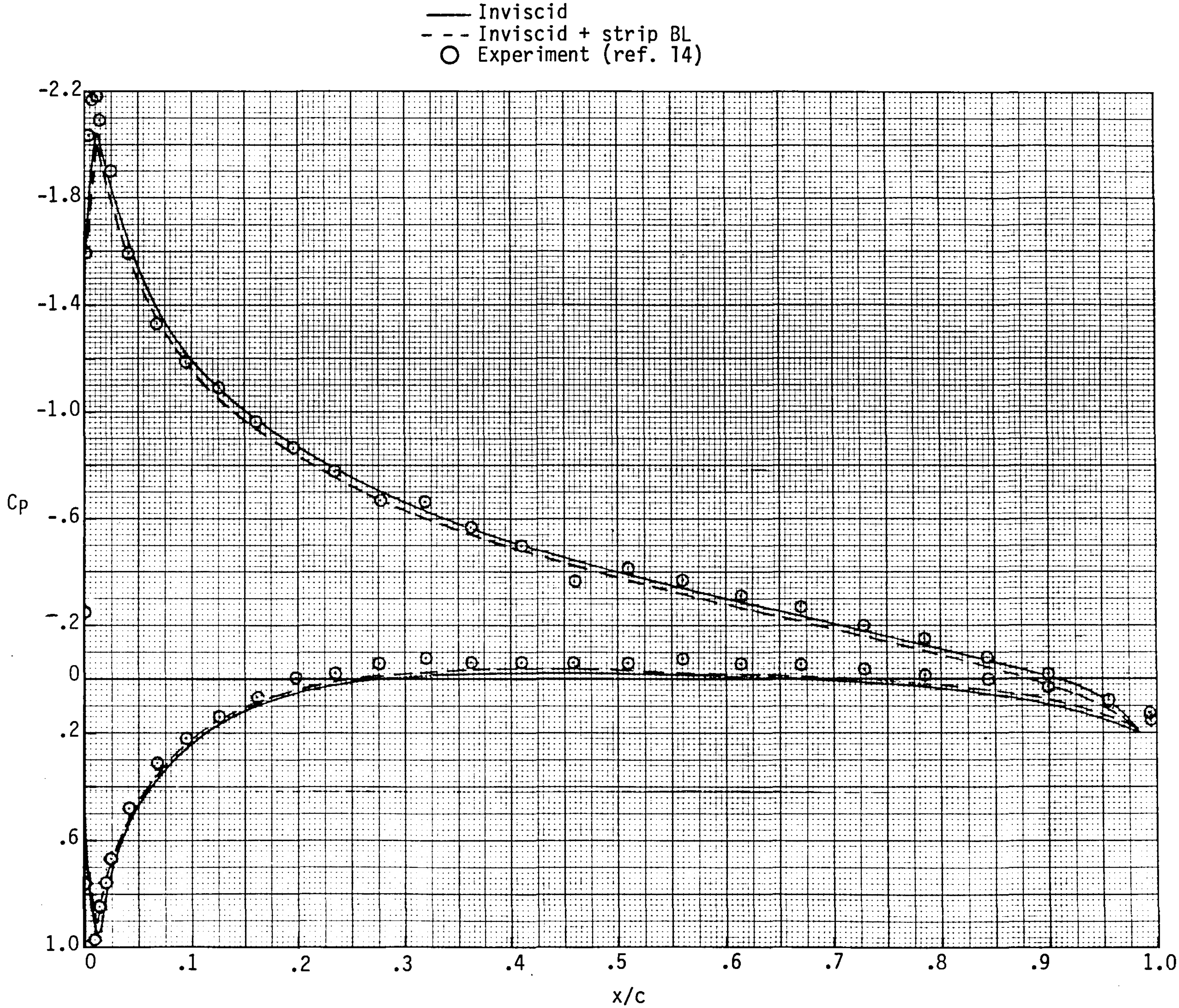

(c) Chordwise pressure distribution. α = 6.75°; η = 0.48

Figure 4.- Concluded.

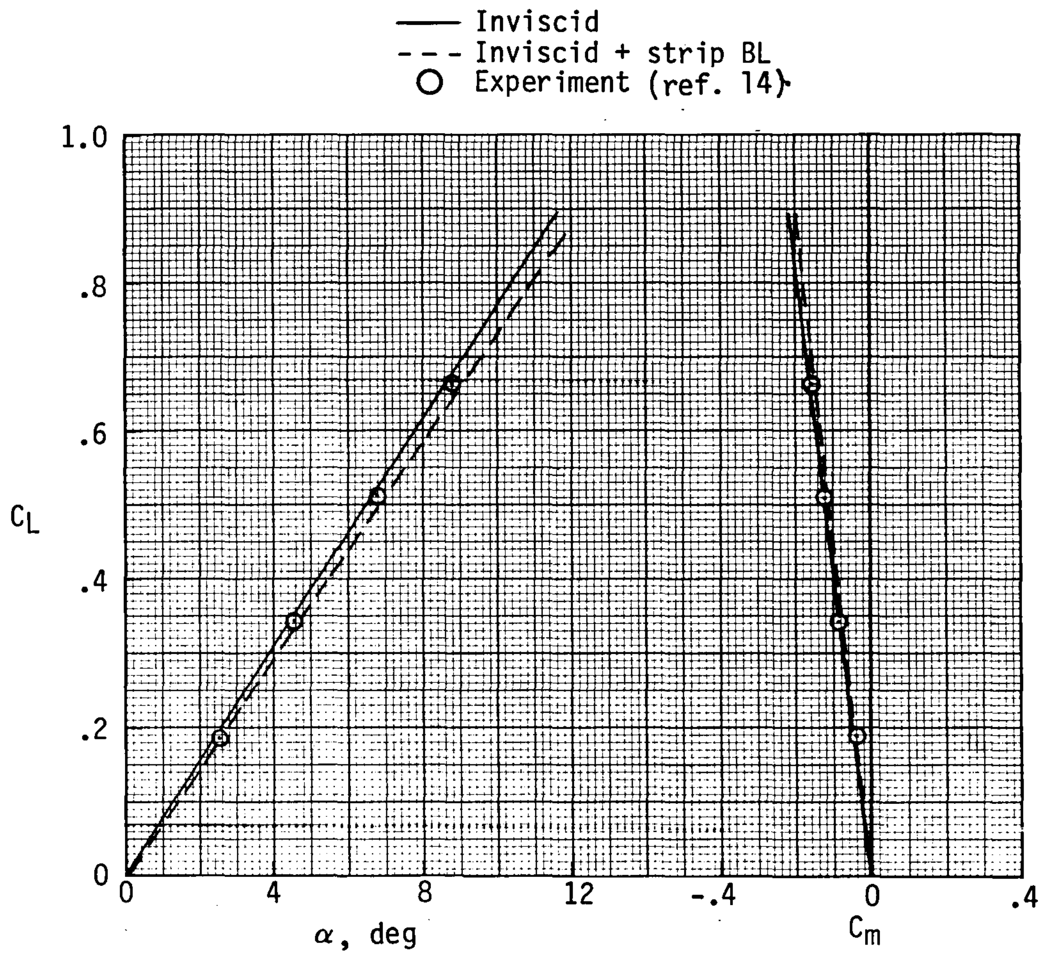

(a) Total lift and pitching moment characteristics

Figure 5.- Comparisons with experiment of wing-alone results using the inviscid method of reference 6 and the two-dimensional boundary layer method of reference 4. $M = .1$; $R_N = 3.2 \times 10^6$.

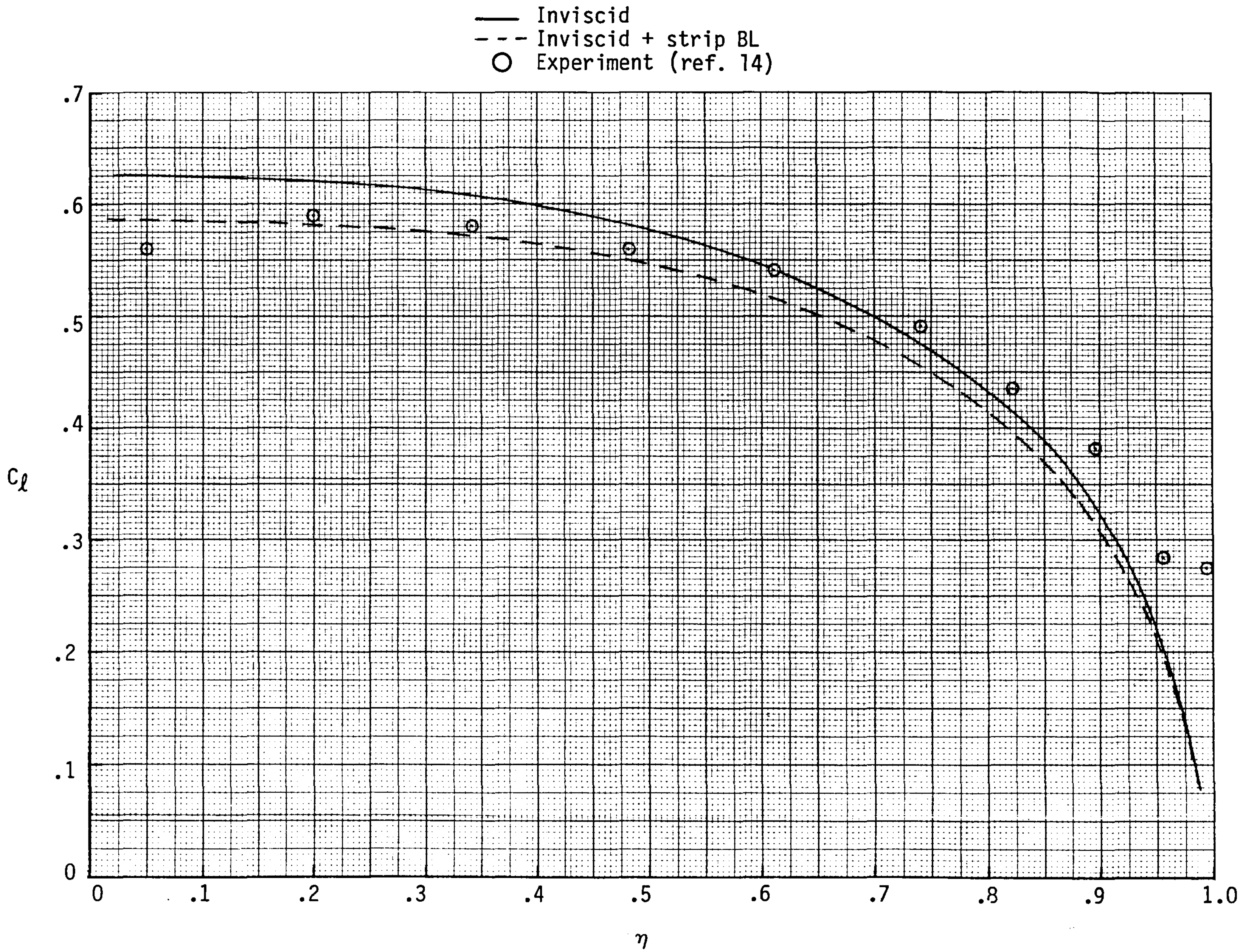

(b) Spanwise load variation, $\alpha = 6.75^o$
Figure 5.- Continued.

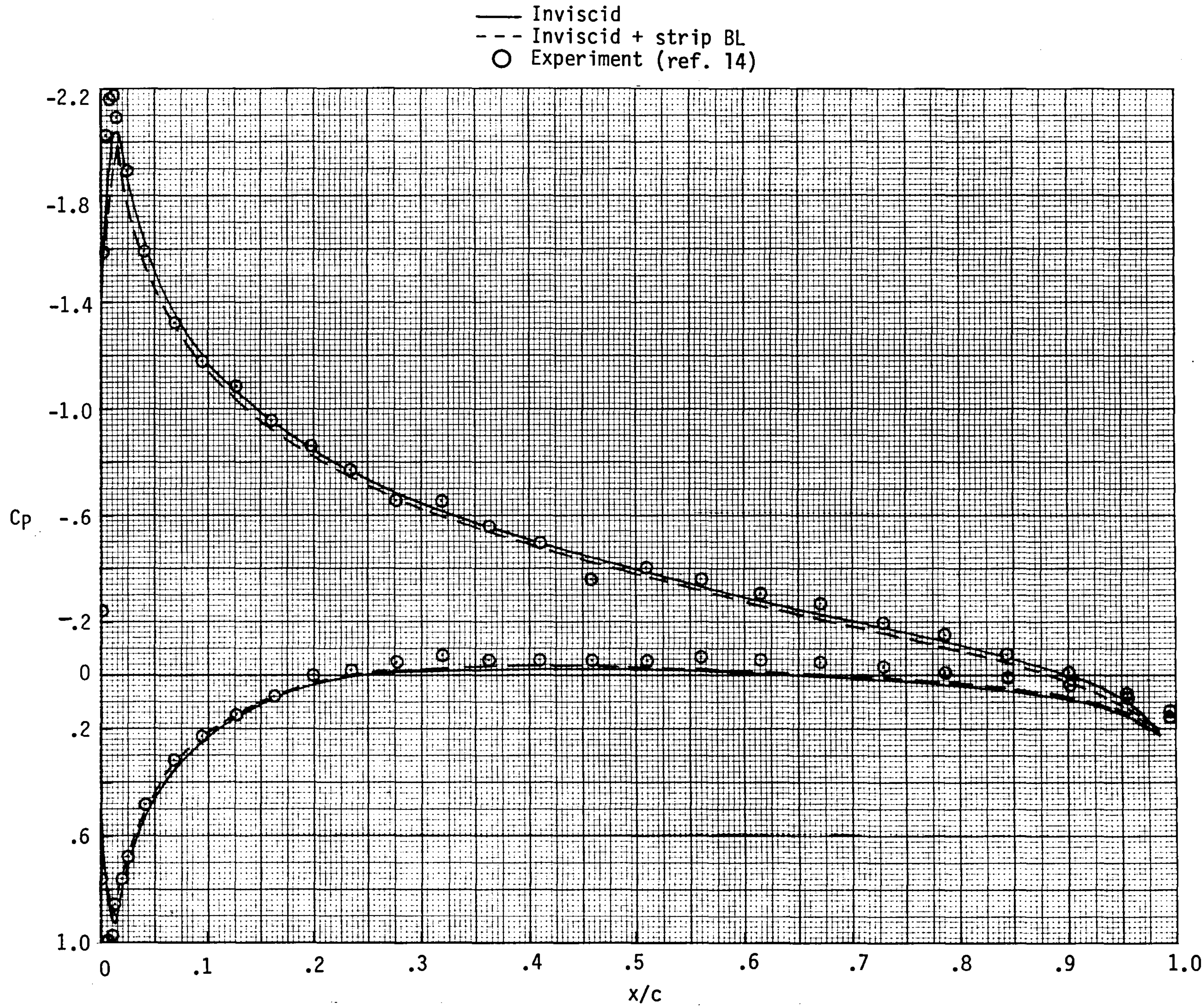

(c) Chordwise pressure distribution, $\alpha = 6.75^{0}$, $\eta = 0.48$

Figure 5.- Concluded.

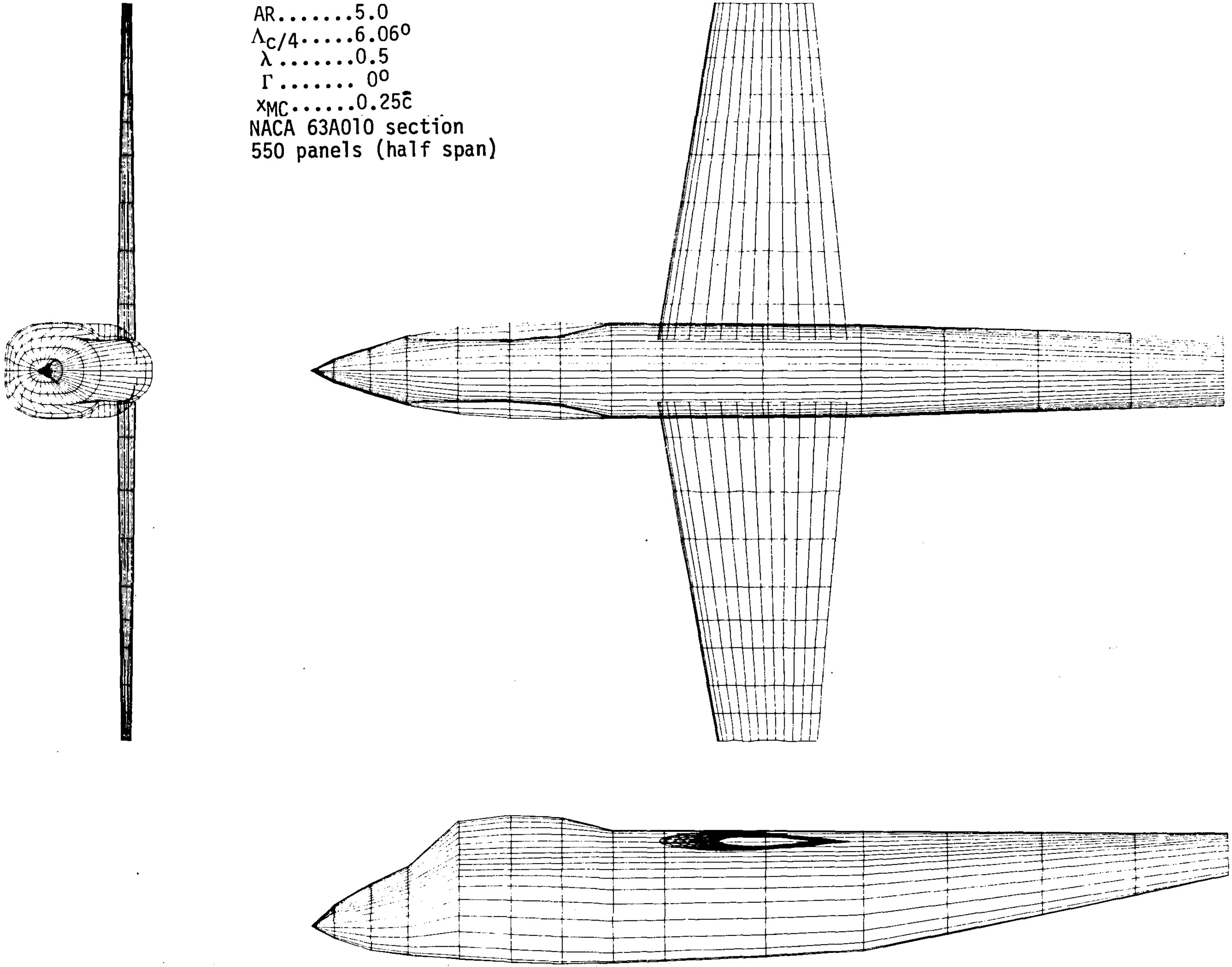

Figure 6.- Three-view of full-span panel representation of wing-body tested in references 15 and 16.

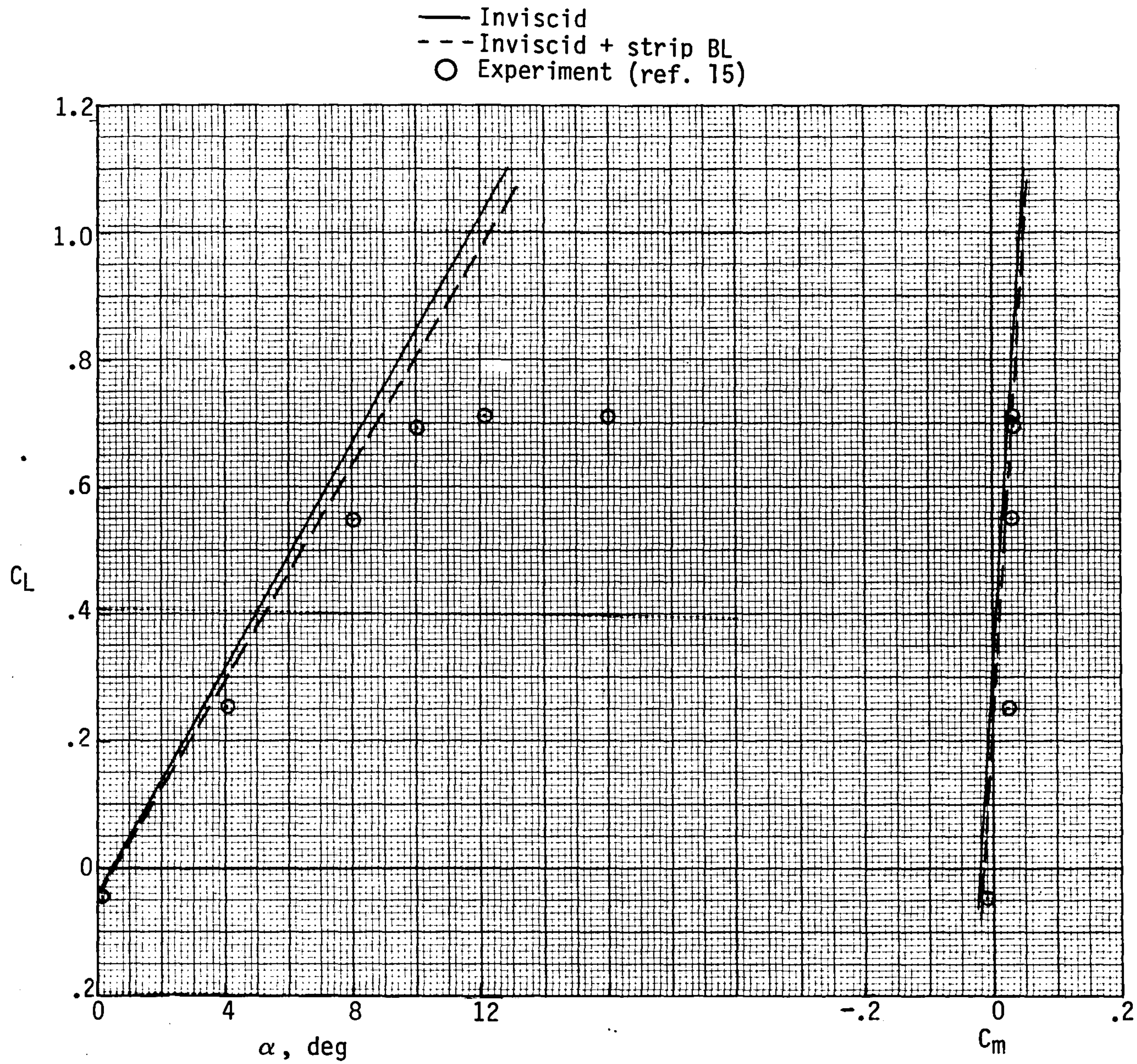

(a) Total lift and pitching moment characteristics

Figure 7.- Comparisons with experiment of wing-body results using the method of reference 1. $M = 0.2$; $R_N = 1.1 \times 10^6$.

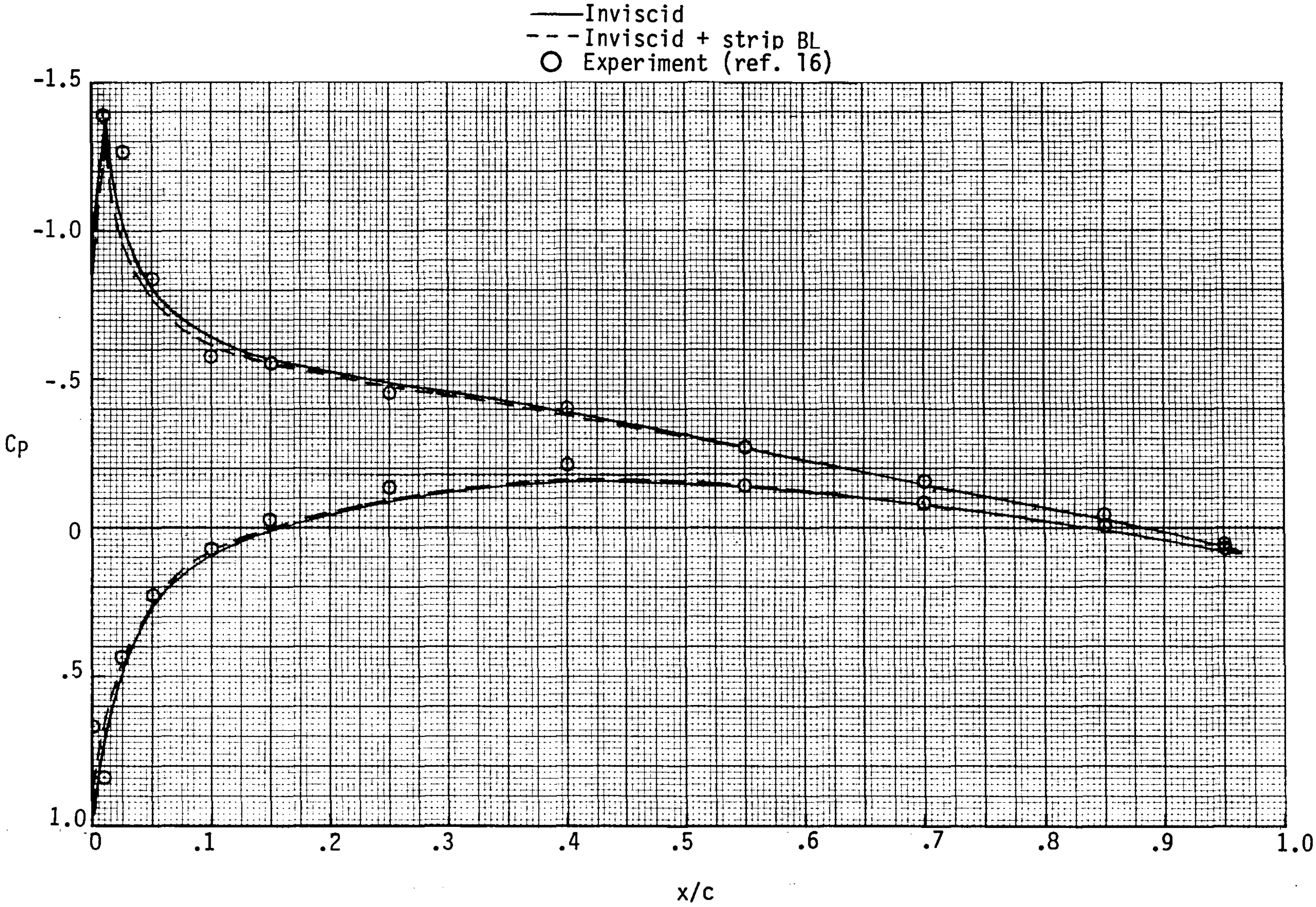

(b) Chordwise pressure distribution, $\alpha = 4.0^{\circ}$, $\eta = 0.25$

Figure 7.- Continued.

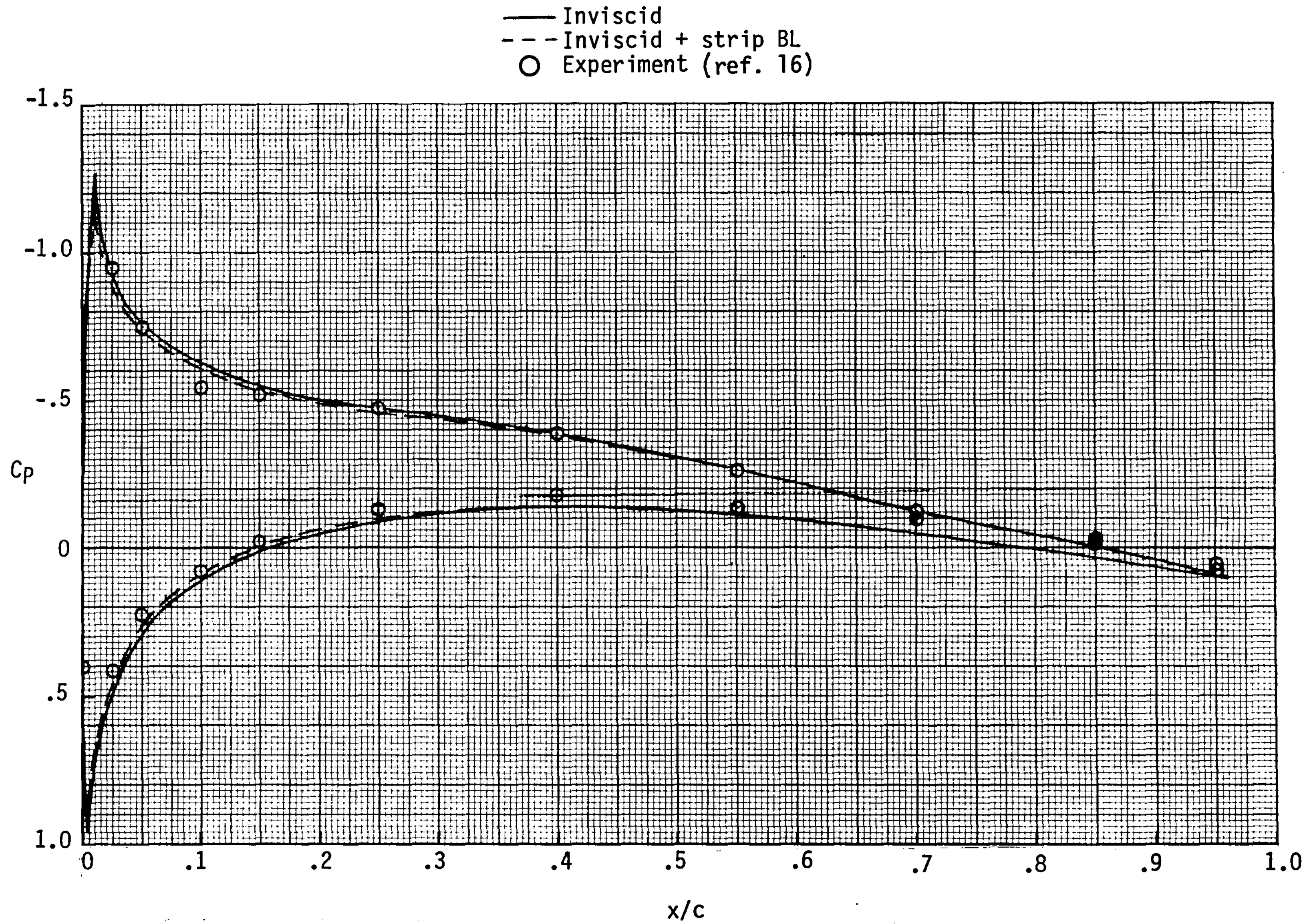

(c) Chordwise pressure distribution, $\alpha = 4.0^{\circ}$, $\eta = 0.80$

Figure 7.- Concluded.

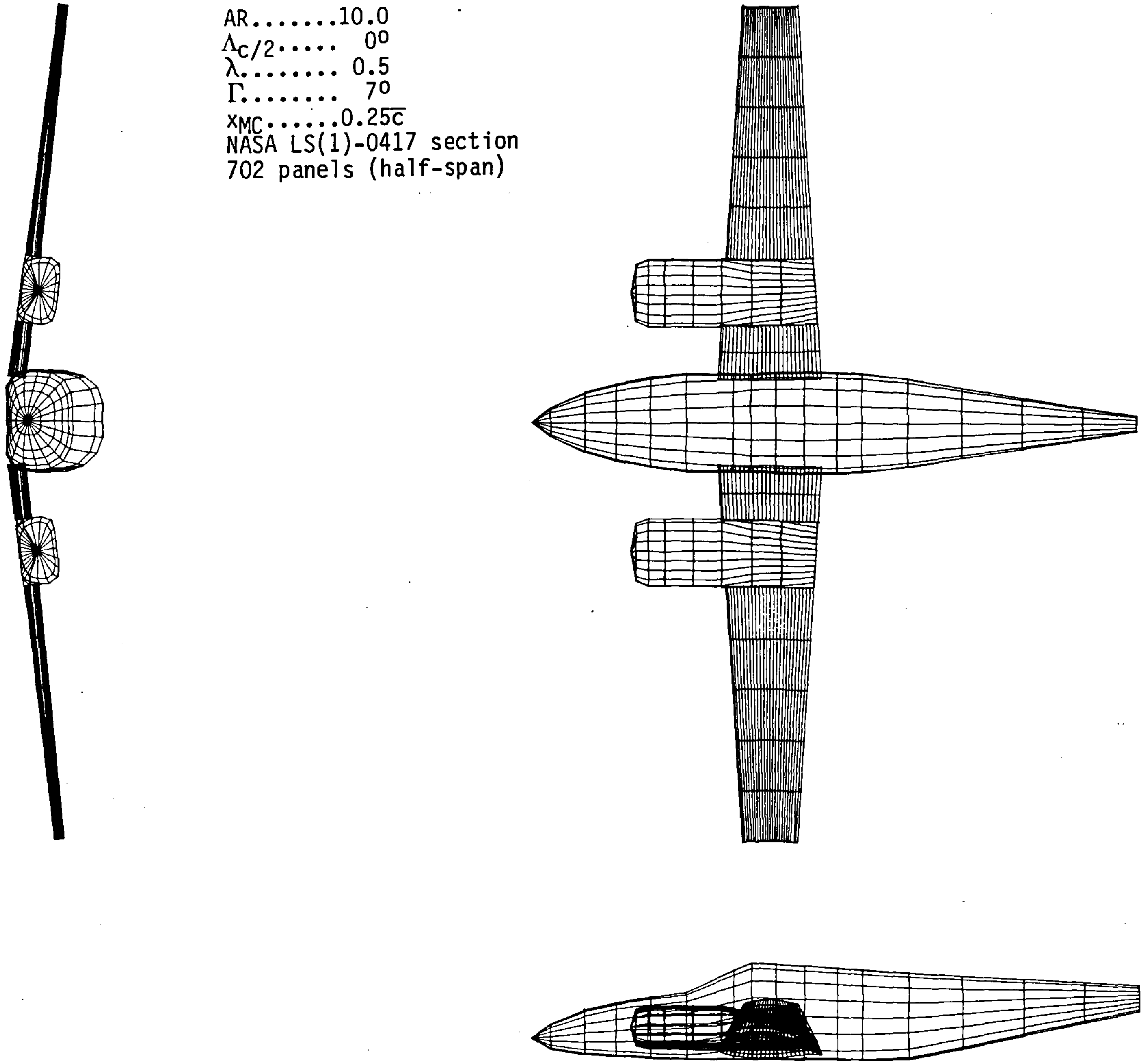

Figure 8.- Three-view of full-span panel representation of ATLIT wing-body-nacelle.

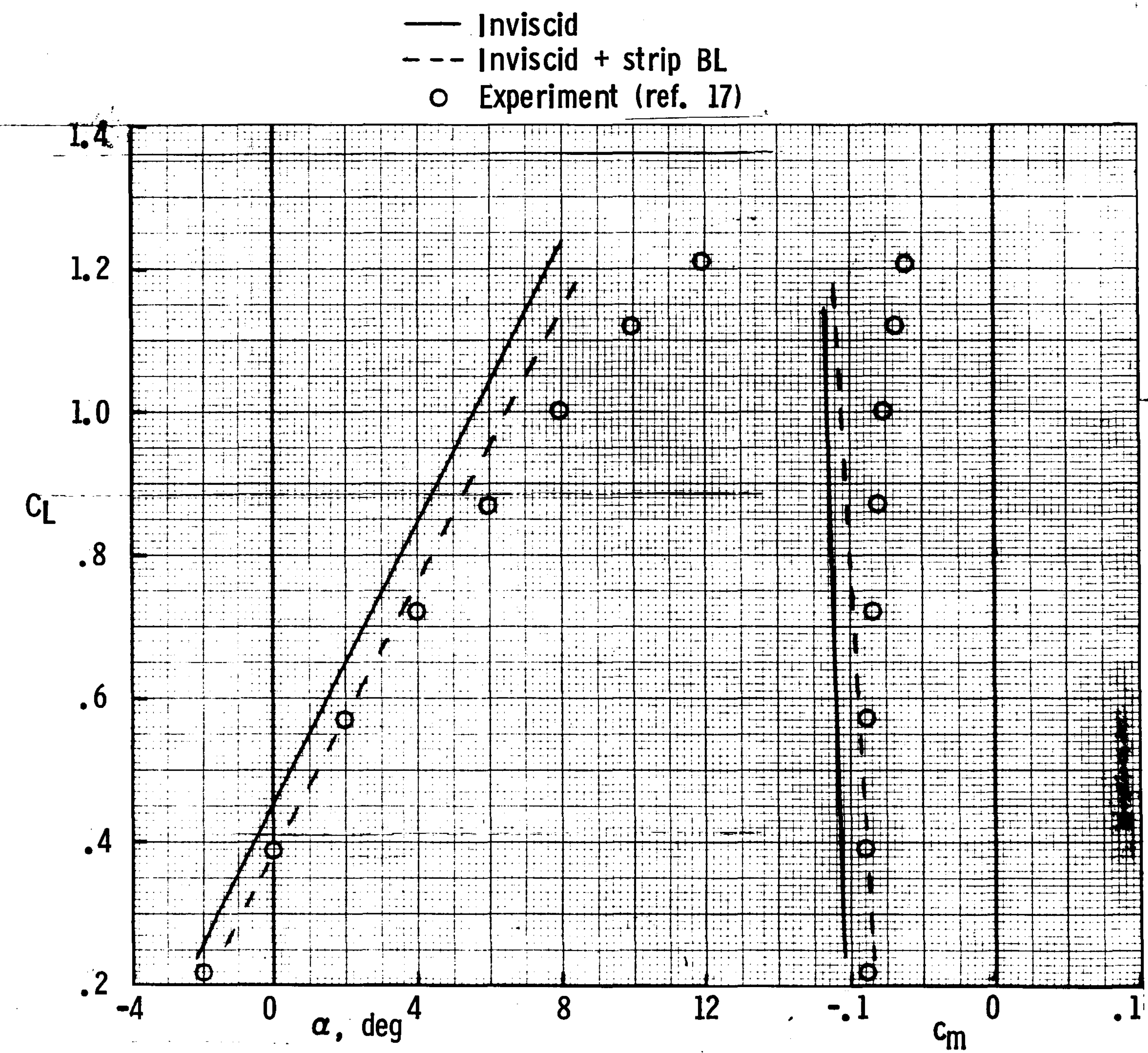

Figure 9.- Comparison with experiment of wing-alone results using the method of reference 1; $M = 0.1$; $R_N = 1.0 \times 10^6$.

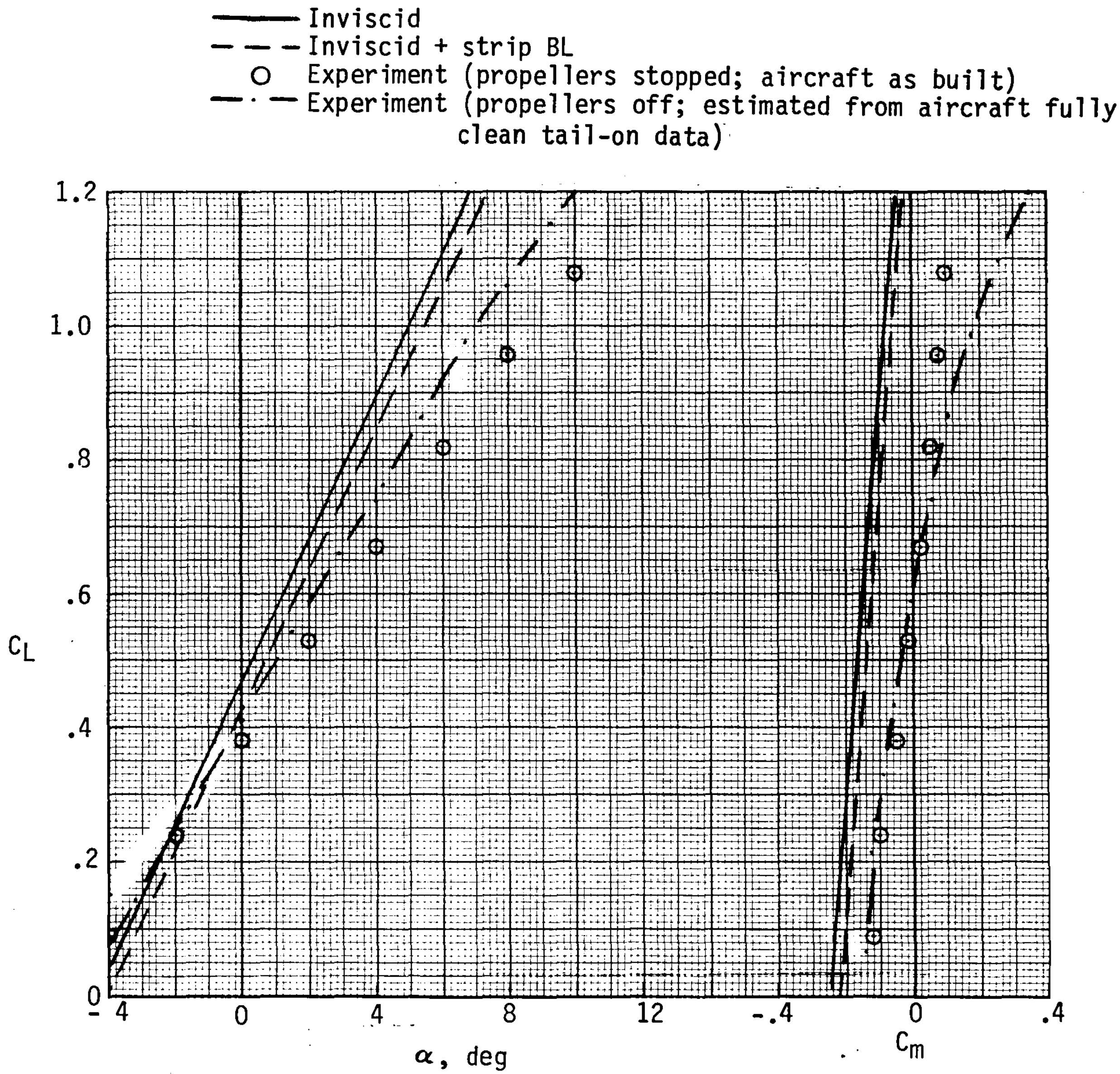

(a) Total lift and pitching moment characteristics

Figure 10.- Comparisons with experiment of wing-body nacelle result using the method of reference 1. $M = 0.1$; $R_N = 3.5 \times 10^6$.

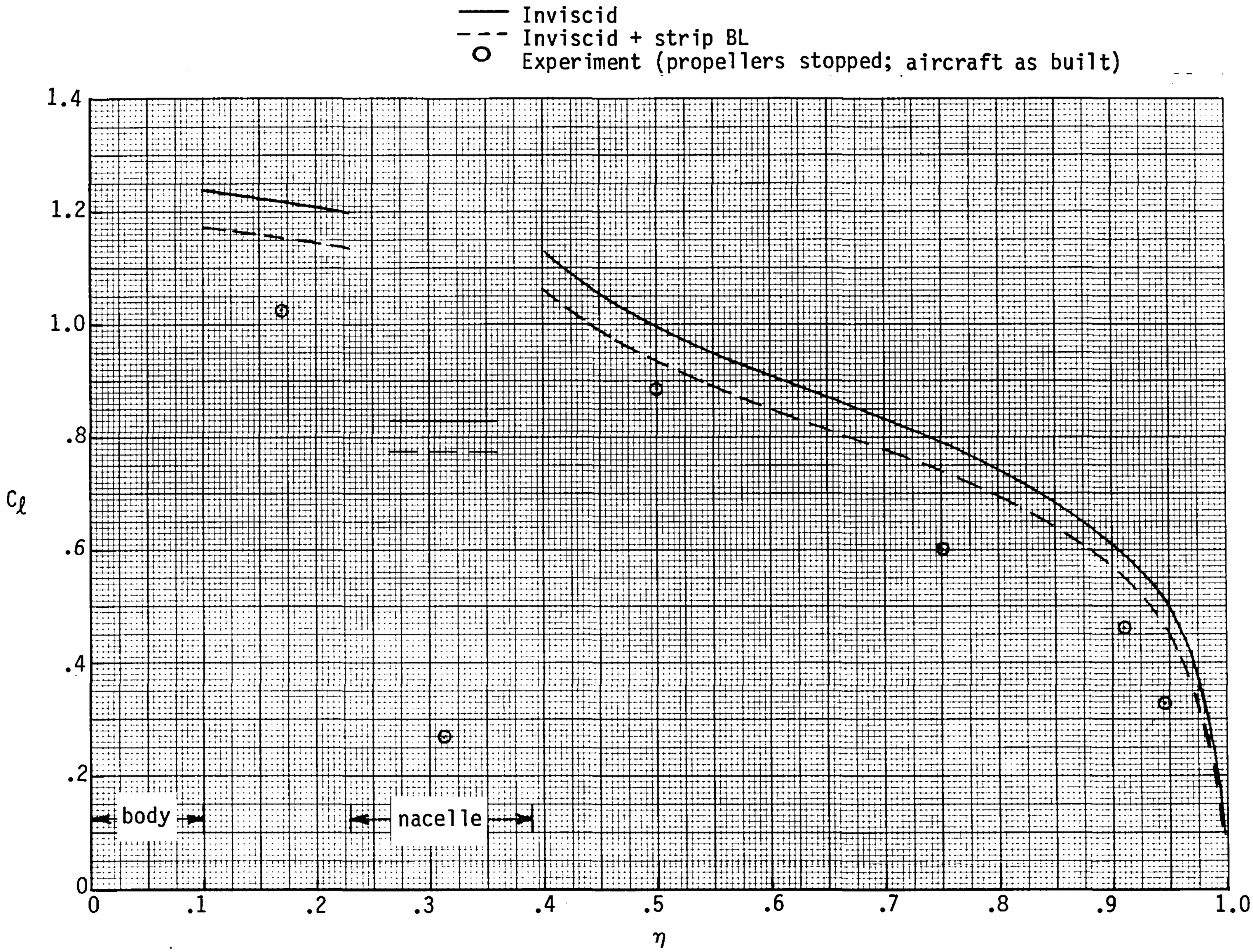

(b) Spanwise load distribution, $\alpha = 4.0^{\circ}$

Figure 10.- Continued.

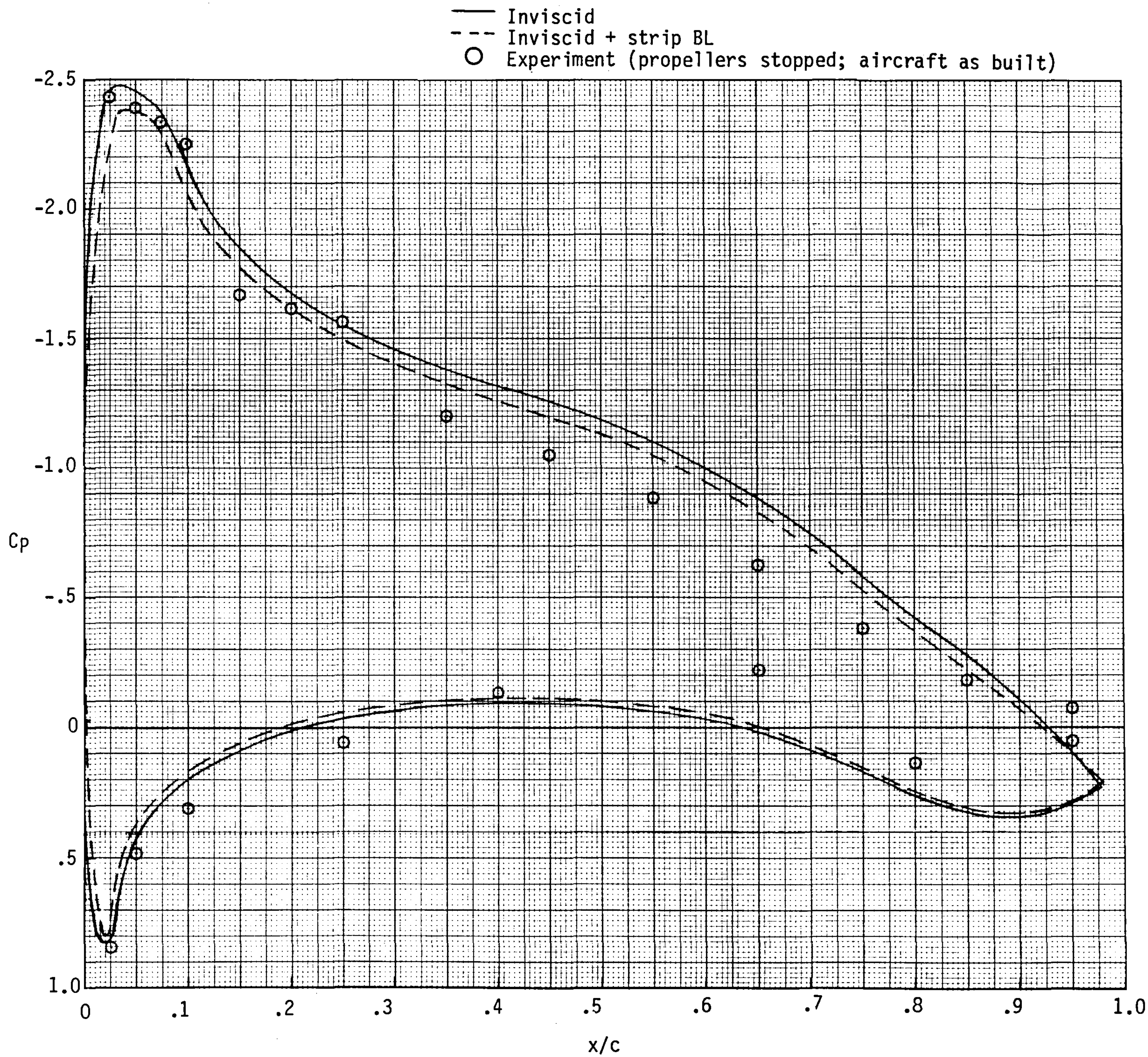

(c) Chordwise pressure distribution, $\alpha = 4.0^{o}$, $\eta = 0.17$

Figure 10.- Continued.

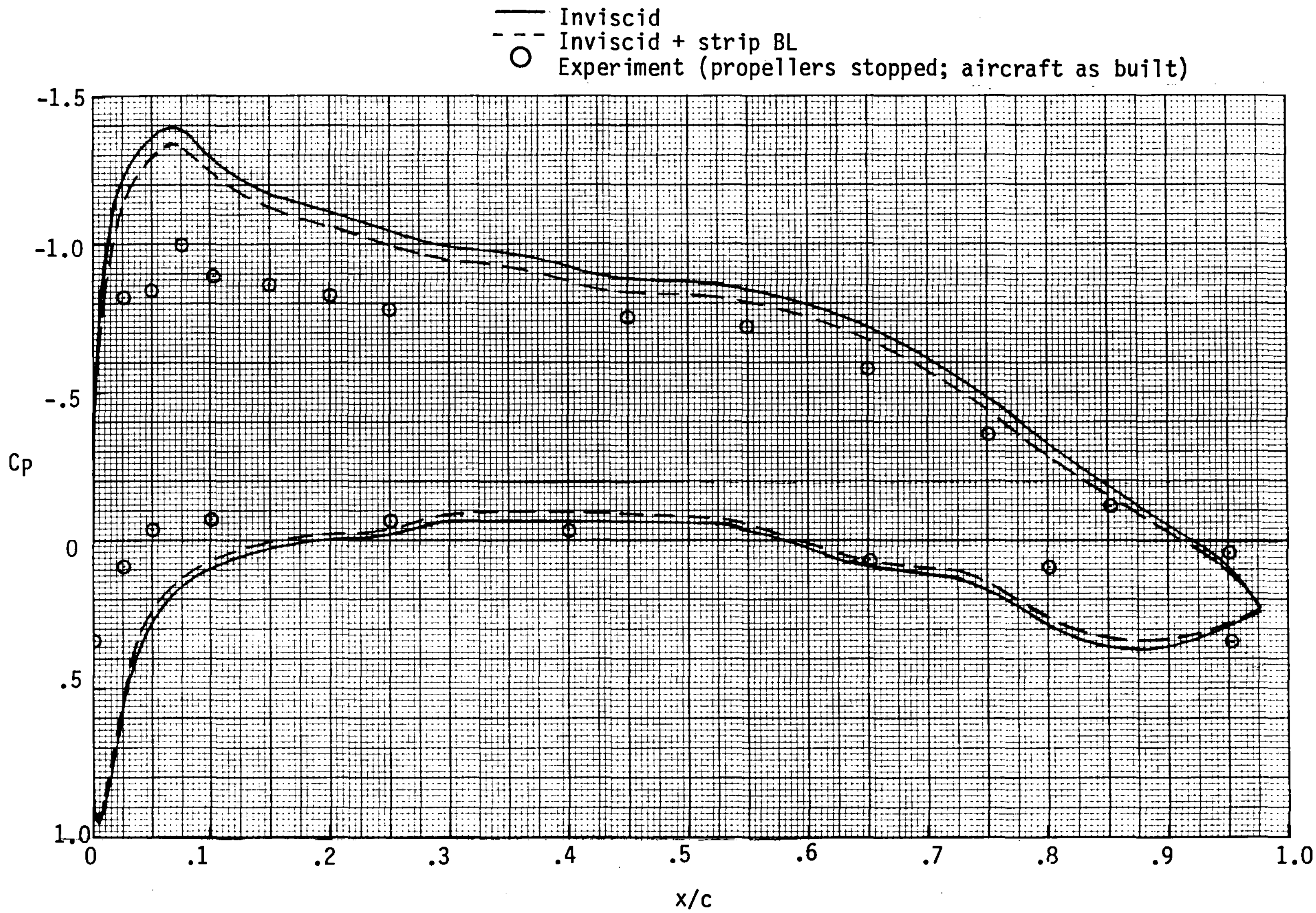

(d) Chordwise pressure distribution, $\alpha = 4.0^{o}$, $\eta = 0.75$

Figure 10.- Concluded.

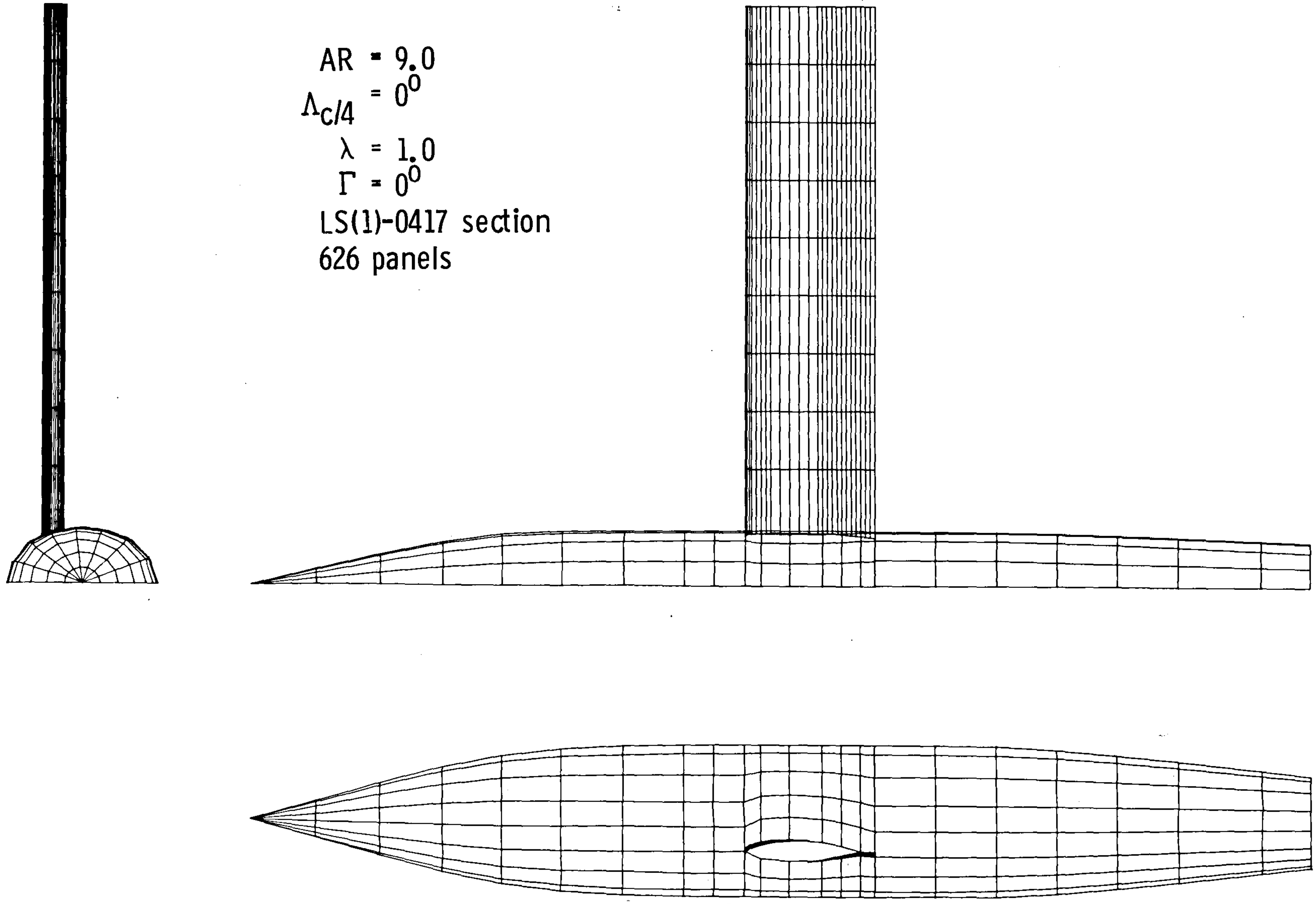

(a) Three-view of half-span panel representation of wing-body

Figure 11.- Comparison with experiment of wing-body result using the method of reference 1; $M = 0.1$; $R_N = 1.4 \times 10^6$.

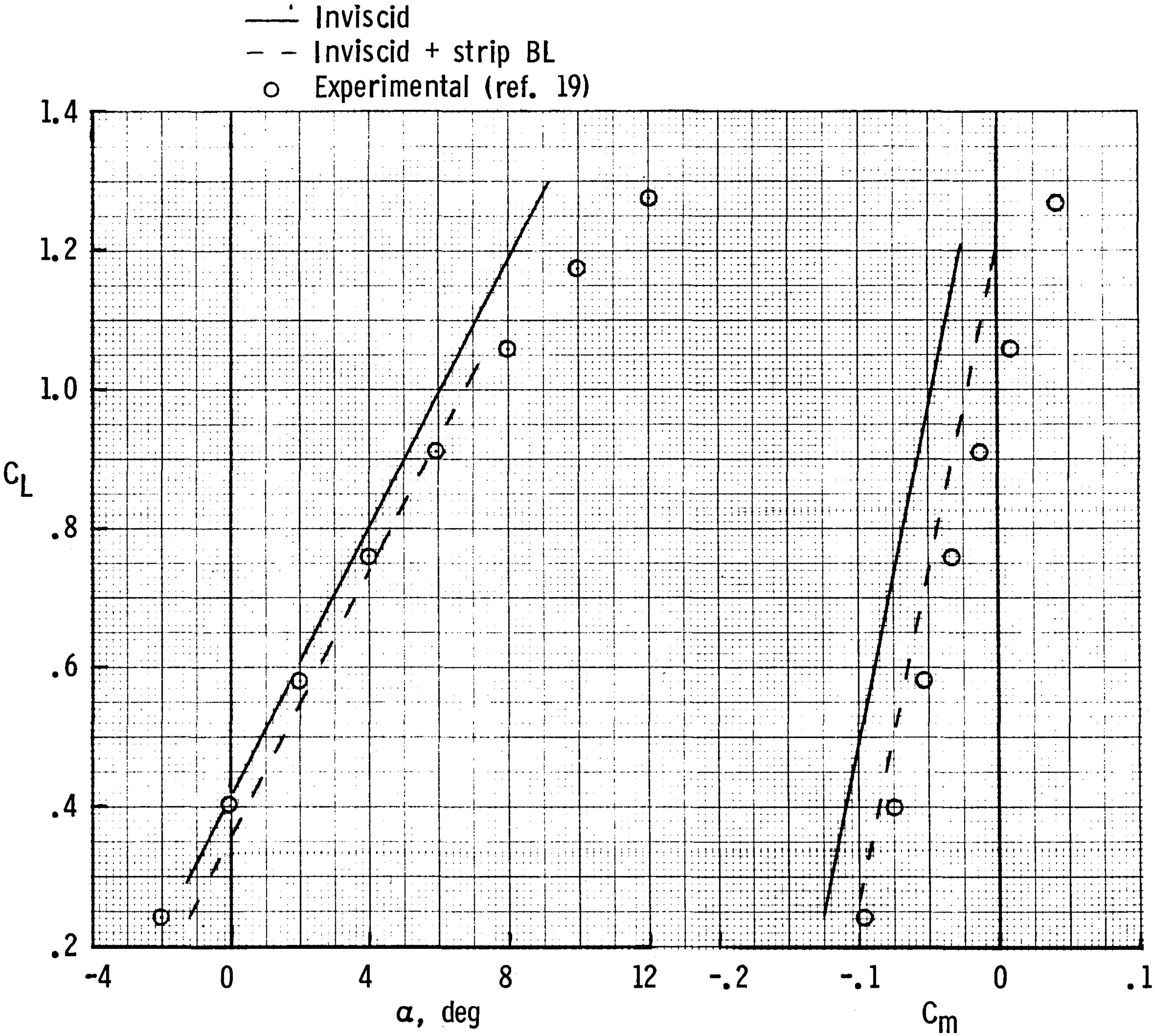

(b) Total lift and moment comparisons

Figure 11.- Concluded.

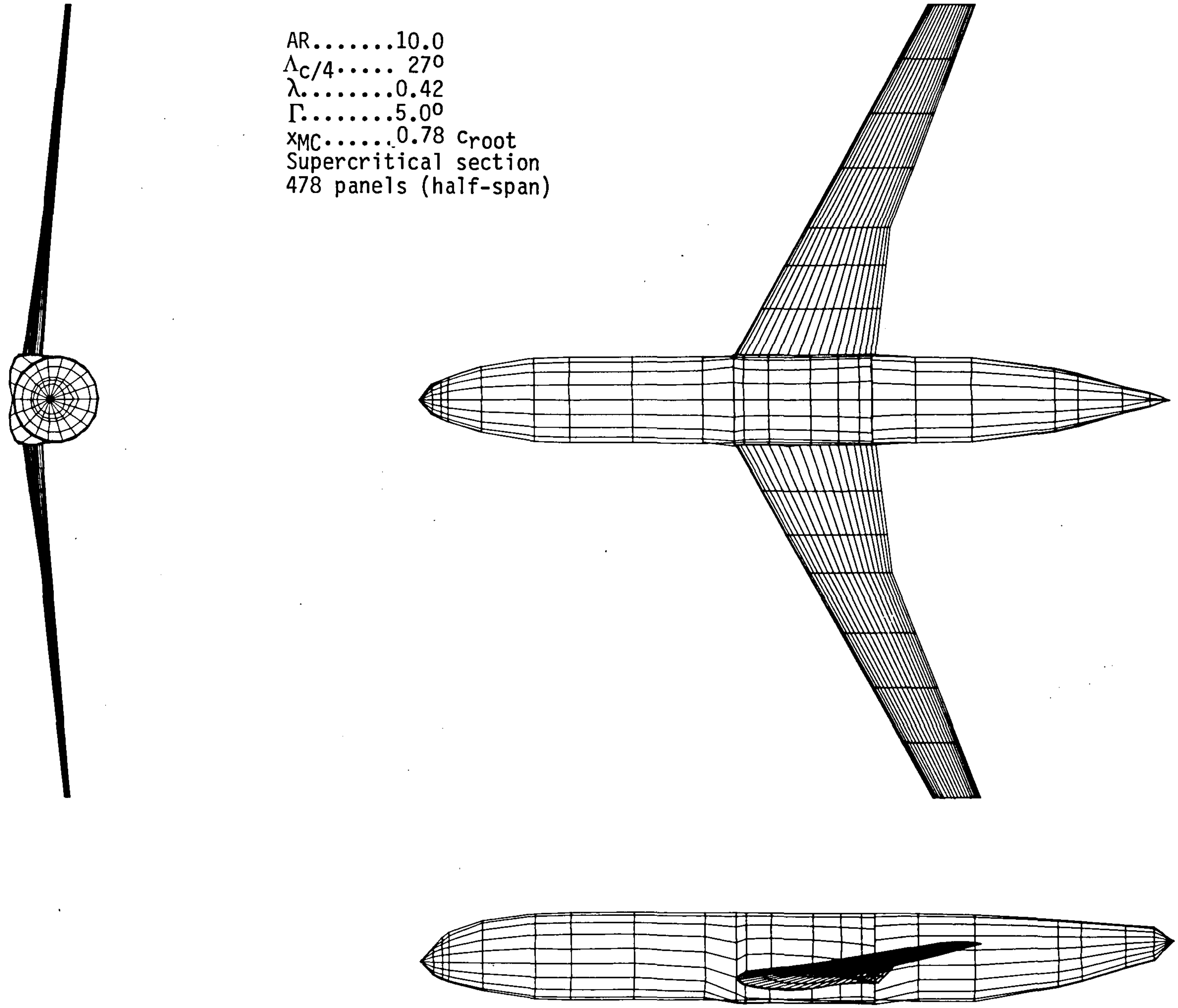

Figure 12.- Three-view of full-span panel representation of EET wing-body configuration tested in reference 20.

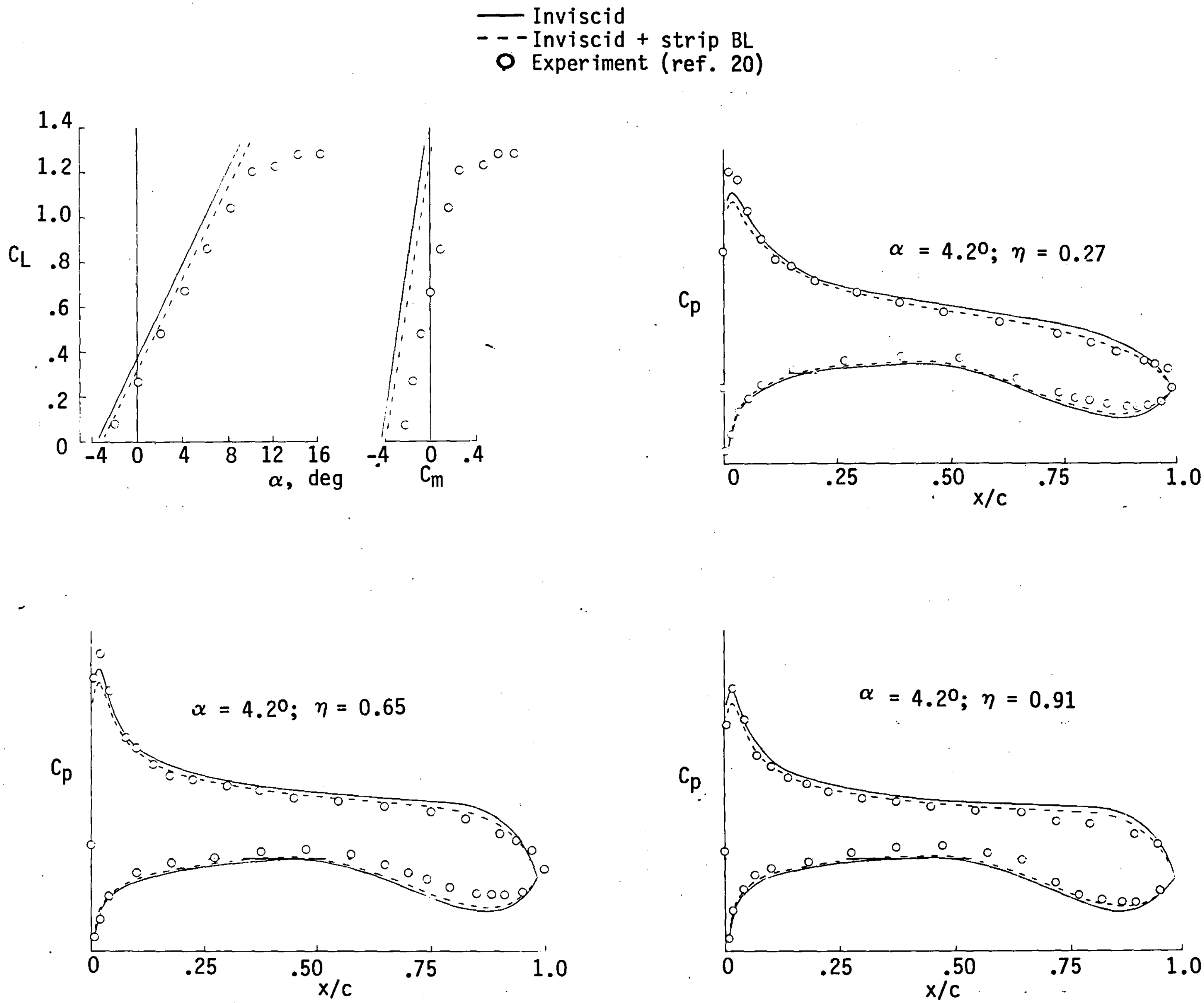

Figure 13.- Comparison with experiment of wing-body results using the method of reference 1. $M = 0.2$; $R_N = 1.4 \times 10^6$.

AR.......12.0
$\Lambda_{c/4}$.....27^{o}
λ........0.33
Γ........5.0^{o}
x_{MC}......0.78 c_{root}
Supercritical section
686 panels (half-span)

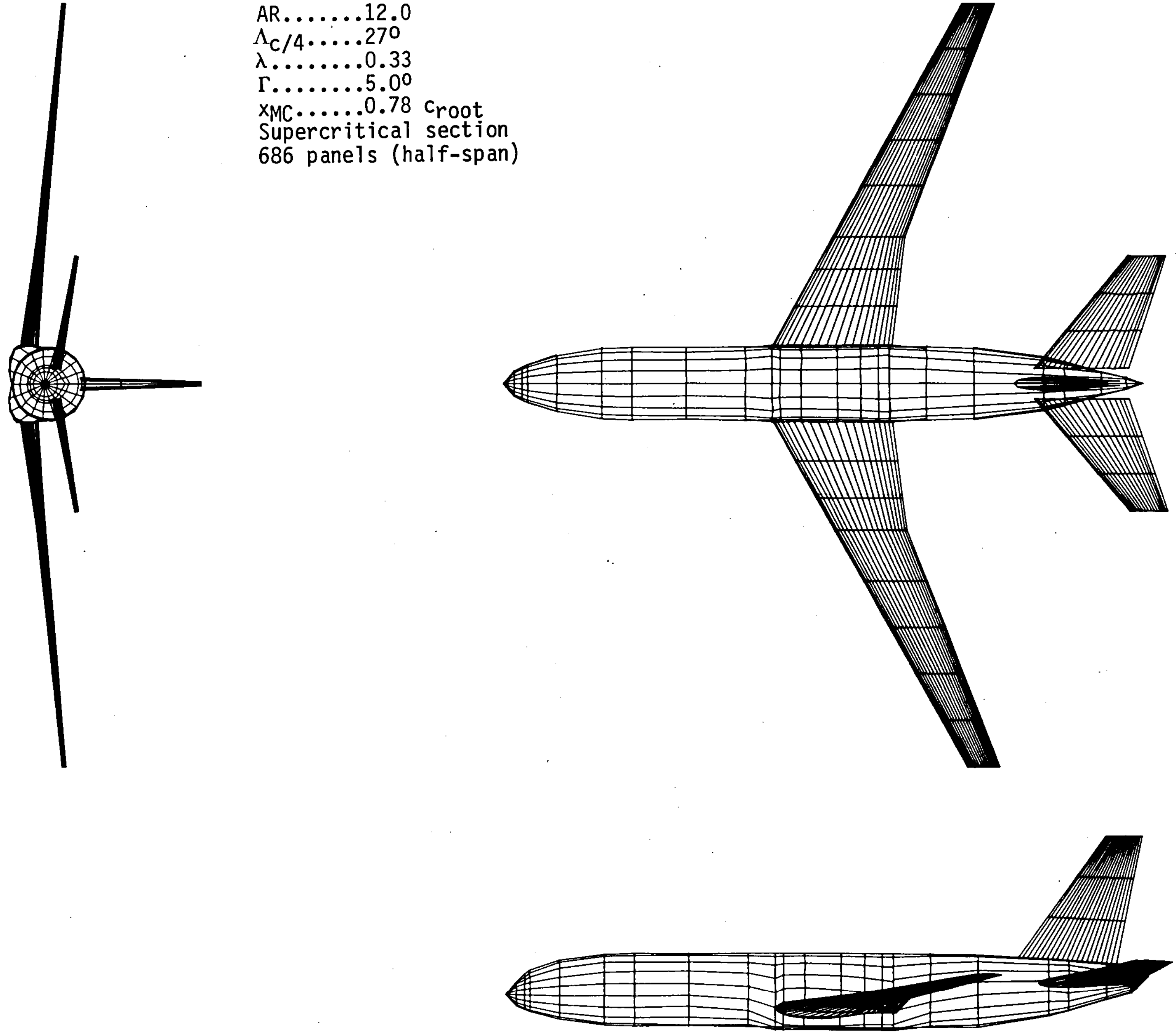

Figure 14.- Three-view of full-span panel representation of EET wing-body-tail tested in reference 20.

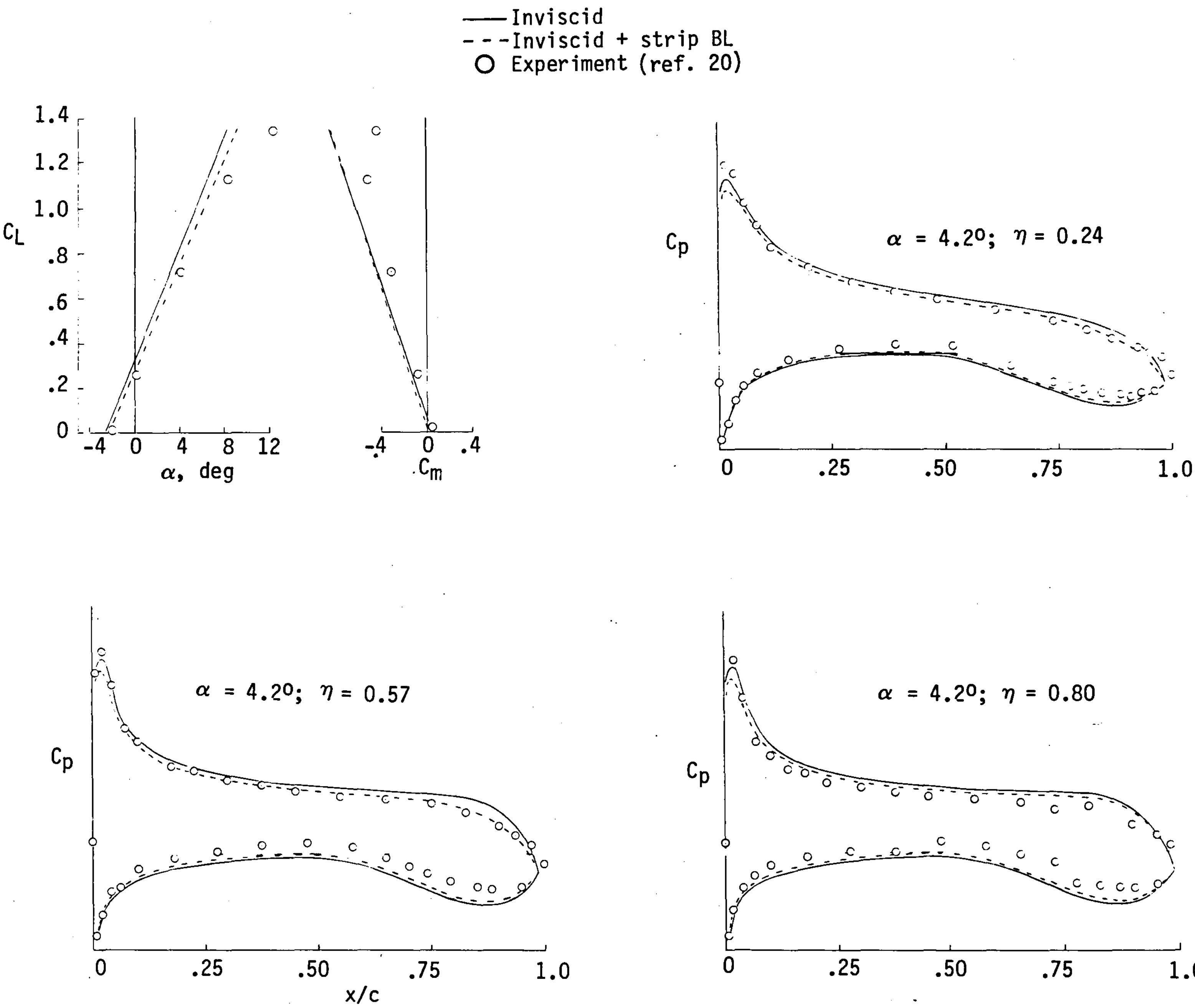

Figure 15.- Comparison with experiment of wing-body-tail results using the method of reference 1. $M = 0.2$; $R_N = 1.4 \times 10^6$.

1. Report No.	2. Government Accession No.	3. Recipient's Catalog No.
TM 80088		

4. Title and Subtitle	5. Report Date
COMPARISON OF THREE-DIMENSIONAL PANEL METHODS WITH STRIP BOUNDARY-LAYER SIMULATIONS TO EXPERIMENT	July 1979
	6. Performing Organization Code
7. Author(s)	8. Performing Organization Report No.
Scott O. Kjelgaard and James L. Thomas	
9. Performing Organization Name and Address	10. Work Unit No.
NASA Langley Research Center Hampton, VA 23665	505-06-53-03
	11. Contract or Grant No.
12. Sponsoring Agency Name and Address	13. Type of Report and Period Covered
National Aeronautics and Space Administration Washington, DC 20546	Technical Memorandum
	14. Sponsoring Agency Code

15. Supplementary Notes

16. Abstract

The results from several three-dimensional surface panel methods coupled on a streamwise strip basis to two-dimensional boundary-layer methods have been compared to experimental data. Several different boundary-layer simulations were investigated; the results indicated that either a transpiration or camber-line displacement simulation gave comparable boundary-layer effects which converged to the expected two-dimensional result with increasing aspect ratio. The method was applied to several varied configurations for which, in general, the lift predictions agreed well with an approximate method based on correcting the inviscid lift using the two-dimensional section viscous characteristics. The wing pressures and the effect of the boundary layer on the wing pressures were predicted accurately.

17. Key Words (Suggested by Author(s))	18. Distribution Statement
Panel methods Boundary layer Potential flow Viscous simulations	Unclassified - Unlimited Subject Category 02

19. Security Classif. (of this report)	20. Security Classif. (of this page)	21. No. of Pages	22. Price*
Unclassified	Unclassified	49	$4.50

* For sale by the National Technical Information Service, Springfield, Virginia 22161

End of Document